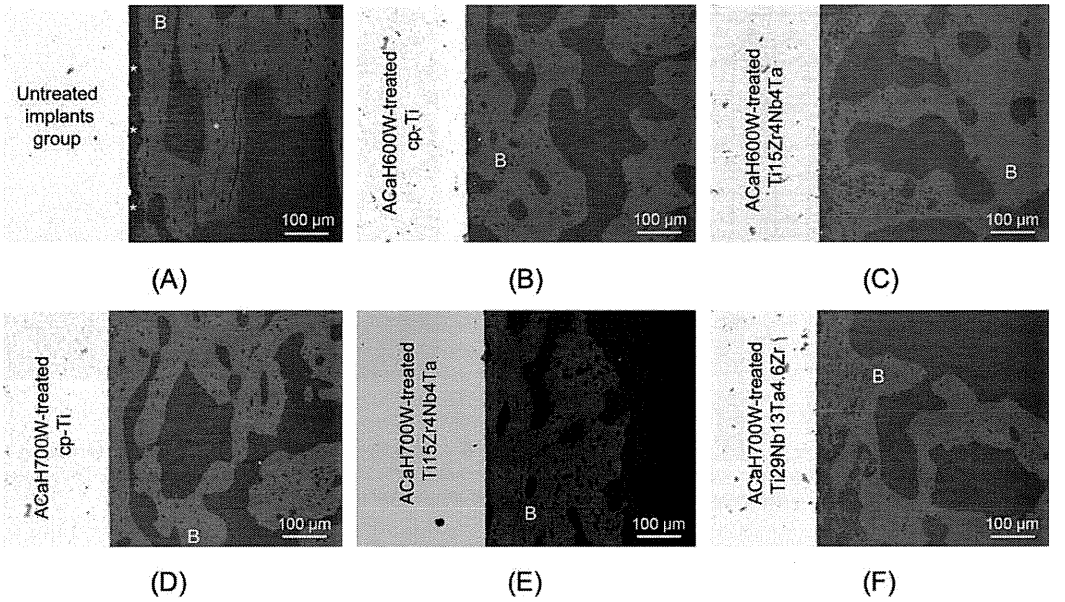

Fig. 6. SEM image (obtained in backscattered mode) of the implant–bone interface at 4 weeks. (A) Untreated implant group. Although immature bone approached the implant, it did not directly bond with the implant, giving rise to a gap (white asterisks) between the implant and the bone. (B) ACaH600W-treated cp-Ti plates. (C) ACaH600W-treated Ti15Zr4Nb4Ta plates. (D) ACaH700W-treated cp-Ti plates. (E) ACaH700W-treated Ti15Zr4Nb4Ta plates. (F) ACaH700W-treated Ti29Nb13Ta4.6Zr plates. Direct bonding between bone and implant was observed for all treated implants. The contact area was comparatively large (D, E) and the new bone was relatively mature and dense. B, bone.

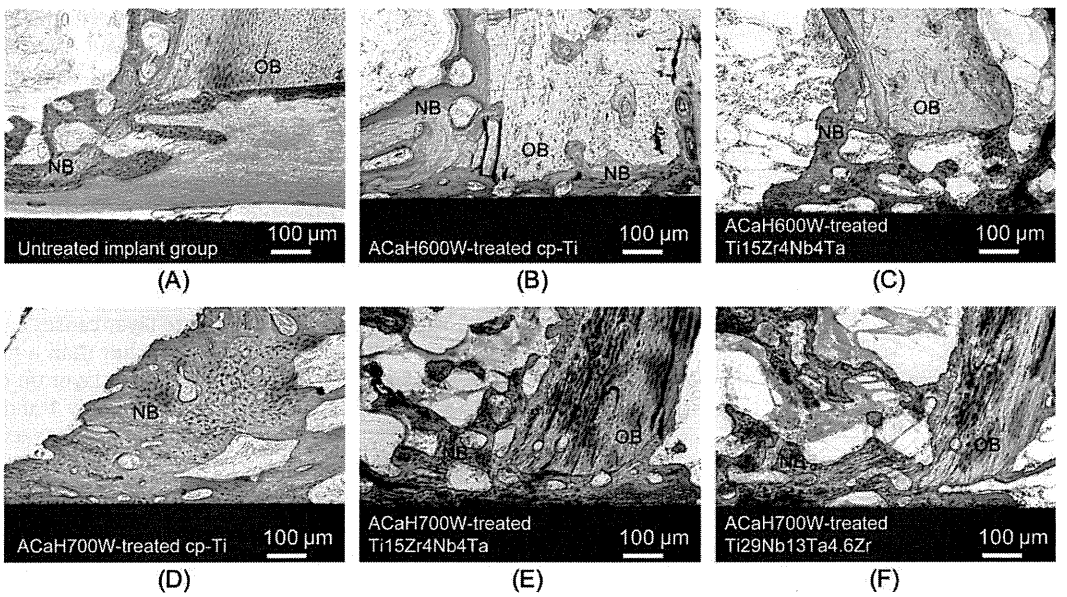

Fig. 7. Surface staining of the bone–implant interface with Stevenel's blue and Van Gieson's picrofuchsin at 4 weeks. (A) Untreated implant group. (B) ACaH600W-treated cp-Ti plates. (C) ACaH600W-treated Ti15Zr4Nb4Ta plates. (D) ACaH700W-treated cp-Ti plates. (E) ACaH700W-treated Ti15Zr4Nb4Ta plates. (F) ACaH700W-treated Ti29Nb13Ta4.6Zr plates. Both the treated and untreated implant groups showed coarse bone formation on the implant. The treated implants (B–F) showed partial direct bone bonding, whereas the untreated implant (A) showed a thick layer of intervening fibrous tissue. The ACaH700W-treated cp-Ti plates (D) had an unclear boundary between the new bone and original bone, which indicated bone maturity. OB, original bone; NB, new bone.

conventional alkali and heat treatment, although successful with Al- and V-containing Ti alloys (Ti6Al4V, Ti15Mo5Zr3Al, and Ti6Al2Nb1Ta) [9–11], was ineffective with Ti15Zr4Nb4Ta and Ti29Nb13Ta4.6Zr.

The increased apatite formation after the NaOH and heat treatments is attributed to the formation of sodium titanate on the surface. In SBF sodium titanate releases Na^+ ions via exchange with H_3O^+ ions to form Ti–OH groups on the surface, which induce apatite formation, as earlier described for NaOH- and heat-treated Ti metal [28,29]. However, Ti containing Ca^{2+} ions instead of Na^+ ions on its surface is expected to exhibit higher apatite formation, since the released Ca^{2+} ions more effectively increase the ionic activity product of the apatite in the surrounding body fluids [30]. In fact, several studies have investigated the incorporation of Ca^{2+} ions onto Ti surfaces [31–33]. However, the techniques mentioned in these studies require expensive specialized apparatus for ion implantation [32] or a specialized high pressure apparatus operating in an aqueous environment at high temperatures for application to medical devices [31,33]. We recently ascertained the in vitro apatite forming ability of cp-Ti, Ti15Zr4Nb4Ta, and

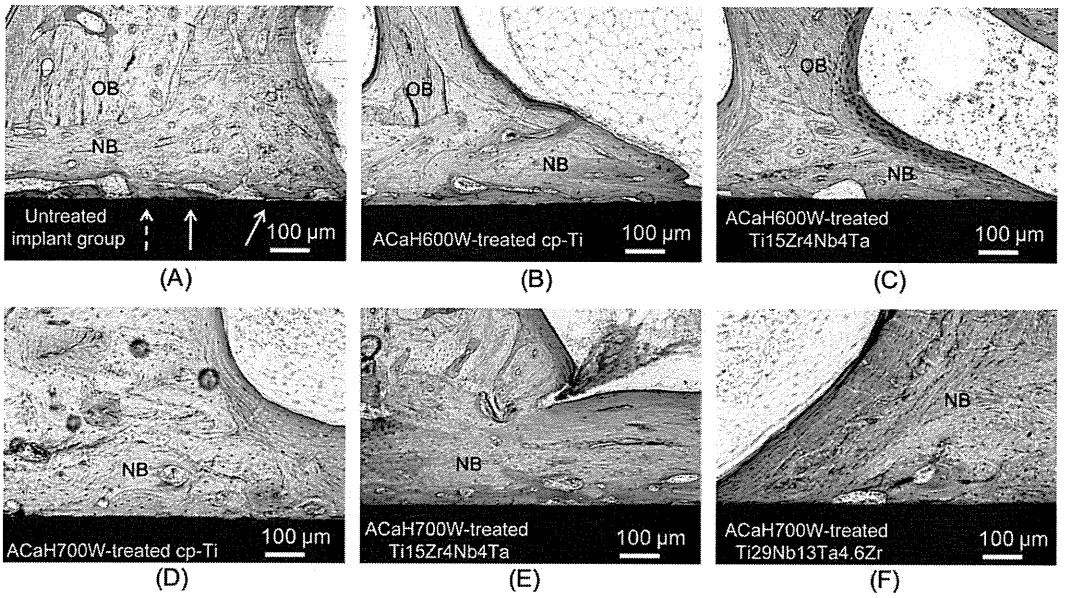

Fig. 8. Surface staining of the bone–implant interface with Stevenel's blue and Van Gieson's picrofuchsin at 16 weeks. (A) Untreated implant group. (B) ACaH600W-treated cp-Ti plates. (C) ACaH600W-treated Ti15Zr4Nb4Ta plates. (D) ACaH700W-treated cp-Ti plates. (E) ACaH700W-treated Ti15Zr4Nb4Ta plates. (F) ACaH700W-treated Ti29Nb13Ta4.6Zr plates. Both the treated and untreated implant groups showed mature bone on the implant. The treated implants (B–F) showed almost complete direct bone bonding, whereas the untreated implant (A) showed a thin layer of intervening fibrous tissue (white arrow) and only partial direct bone bonding (dotted white arrow). The ACaH700W-treated samples exhibited new bone of such maturity that the new bone was undistinguishable from the original bone (D–F), although this was not the case with the ACaH600W-treated plates (B, C). OB, original bone; NB, new bone.

Ti29Nb13Ta4.6Zr alloy implants by using simple and economical ACaHW treatments [17–19]. Furthermore, in the present study an in vivo bone bonding ability was confirmed. The mechanisms of apatite formation following ACaHW treatment are interpreted in terms of surface structural changes as follows. The apatite forming ability increased after $CaCl_2$ treatment following NaOH treatment, although this ability is lost after heat treatment to strengthen the treated layer due to the reduced mobility of Ca^{2+} ions in calcium titanate [17]. This problem is resolved by the subsequent water treatment, which contributes to increased mobility of the Ca^{2+} ions in calcium titanate by incorporation of H_3O^+ ions [17].

We previously reported that sodium removal through hot water immersion in the course of alkali and heat treatment considerably enhanced the apatite forming ability of Ti in SBF. Sodium removal enhanced the bone bonding strength of Ti subjected to alkali and heat treatment at 4 and 8 weeks post-operative, however, the failure loads of the implants subjected to sodium-free alkali and heat treatment decreased after 16 weeks implantation because the treated layer flaked off [5]. On the other hand, the failure loads in the present study did not decrease and no flaking of the treated layer was observed by SEM through to the end. We considered that the stability of the ACaHW-treated layer was confirmed by these results.

In comparison with the case of heat treatment at 600 °C, heat treatment at 700 °C led to a significant improvement in apatite formation in SBF and tensile strength in vivo. However, the EDX results were not significantly different. In the detachment test all treated specimens ruptured on the bone side. Hence, we consider that the differences in failure load between samples subjected to ACaH600W and ACaH700W treatment stem from bone maturity and adhesion based on the histological findings. In other words, the increase in heat treatment temperature to 700 °C increased the extent of bone formation around the implant.

In general, the apatite forming ability of Ti metal subjected to alkali and heat treatment was liable to decrease when the treated Ti metal was stored in a humid environment for a long period of time, because of the release of Na^+ ions from the sodium titanate. However, it is reported that the apatite forming ability of ACaHW-treated Ti metal did not decrease, even when the treated Ti metal was kept in a humid environment [19]; this finding can be attributed to the low mobility of Ca^{2+} ions compared with Na^+ ions in the titanate.

Thus, from an overall perspective, it is expected that when Ti15Zr4Ta4Nb and Ti29Nb13Ta4.6Zr alloys with superior biocompatibility and mechanical properties are endowed with bioactivity and stability through ACaHW treatment, the treated alloys will be useful in developing novel orthopedic implants that function under loaded conditions, such as cementless joint replacement implants, external fixation pins, and spinal fusion implants.

5. Conclusions

Commercially pure Ti and its Zr-, Nb-, and Ta-containing alloys (without V and Al), namely Ti15Zr4Ta4Nb and Ti29Nb13Ta4.6Zr, exhibit enhanced apatite formation in vitro and bone bonding in vivo after alkali, $CaCl_2$, heat, and water treatment. In particular, implants heat treated at 700 °C have significantly augmented apatite formation in SBF and stronger bone bonding in vivo. The present results suggest that these treated Ti alloys may be useful to develop novel orthopedic implants that function under loaded conditions, because of their superior mechanical properties and excellent bioactivity and cytocompatibility.

Acknowledgements

This work was supported by the Translational Research Promotion Project as part of the Health Assurance Program of the New Energy and Industrial Technology Development Organization (NEDO). We thank Dr. Yoshimitsu Okazaki for supplying the alloy used in the study.

Appendix Appendix. A. Figures with essential colour discrimination

Certain figures in this article, particularly Figs. 1, 7, and 8 are difficult to interpret in black and white. The full colour images

can be found in the on-line version, at doi:10.1016/j.actbio.2010.09.026.

References

[1] Sugino A, Ohtsuki C, Tsuru K, Hayakawa S, Nakano T, Okazaki Y, et al. Effect of spatial design and thermal oxidation on apatite formation on Ti–15Zr–4Ta–4Nb alloy. Acta Biomater 2009;5:298–304.

[2] Kasuga T, Nogami M, Niinomi M, Hattori T. Bioactive calcium phosphate invert glass-ceramic coating on beta-type Ti–29Nb–13Ta–4.6Zr alloy. Biomaterials 2003;24:283–90.

[3] De Groot K, Geesink R, Klein C, Serekian R. Plasma sprayed coatings of hydroxyapatite. J Biomed Mater Res 1987;21:1375–81.

[4] Klein CP, Patka P, van der Lubbe HB, Wolke JG, de Groot K. Plasma-sprayed coatings of tetracalciumphosphate, hydroxyl-apatite, and alpha-TCP on titanium alloy: an interface study. J Biomed Mater Res 1991;25:53–65.

[5] Fujibayashi S, Nakamura T, Nishiguchi S, Tamura J, Uchida M, Kim HM, et al. Bioactive titanium: effect of sodium removal on the bone-bonding ability of bioactive titanium prepared by alkali and heat treatment. J Biomed Mater Res 2001;56:562–70.

[6] Takemoto M, Fujibayashi S, Neo M, Suzuki J, Kokubo T, Nakamura T. Mechanical properties and osteoconductivity of porous bioactive titanium. Biomaterials 2005;26:6014–23.

[7] Takemoto M, Fujibayashi S, Neo M, Suzuki J, Matsushita T, Kokubo T, et al. Osteoinductive porous titanium implants: effect of sodium removal by dilute HCl treatment. Biomaterials 2006;27:2682–91.

[8] Kawanabe K, Ise K, Goto K, Akiyama H, Nakamura T, Kaneuji A, et al. A new cementless total hip arthroplasty with bioactive titanium porous-coating by alkaline and heat treatment: average 4.8-year results. J Biomed Mater Res B Appl Biomater 2009;90:476–81.

[9] Kim HM, Miyaji F, Kokubo T, Nakamura T. Preparation of bioactive Ti and its alloys via simple chemical surface treatment. J Biomed Mater Res 1996;32:409–17.

[10] Nishiguchi S, Kato H, Fujita H, Kim HM, Miyaji F, Kokubo T, et al. Enhancement of bone-bonding strengths of titanium alloy implants by alkali and heat treatments. J Biomed Mater Res 1999;48:689–96.

[11] Kim HM, Takadama H, Kokubo T, Nishiguchi S, Nakamura T. Formation of a bioactive graded surface structure on Ti–15Mo–5Zr–3Al alloy by chemical treatment. Biomaterials 2000;21:353–8.

[12] Steinemann S. Corrosion of Surgical Implants – In Vivo and In Vitro Tests. New York: Wiley; 1980.

[13] Hallab NJ, Vermes C, Messina C, Roebuck KA, Glant TT, Jacobs JJ. Concentration- and composition-dependent effects of metal ions on human MG-63 osteoblasts. J Biomed Mater Res 2002;60:420–33.

[14] Niinomi M. Metallic biomaterials. J Artif Organs 2008;11:105–10.

[15] Okazaki Y, Rao S, Ito Y, Tateishi T. Corrosion resistance, mechanical properties, corrosion fatigue strength and cytocompatibility of new Ti alloys without Al and V. Biomaterials 1998;19:1197–215.

[16] Niinomi M. Fatigue performance and cyto-toxicity of low rigidity titanium alloy, Ti–29Nb–13Ta–4.6Zr. Biomaterials 2003;24:2673–83.

[17] Yamaguchi S, Takadama H, Matsushita T, Nakamura T, Kokubo T. Apatite-forming ability of Ti–15Zr–4Nb–4Ta alloy induced by calcium solution treatment. J Mater Sci Mater Med, 2009.

[18] Yamaguchi S, Kizuki T, Takadama H, Matsushita T, Kokubo T, Fukuda A, et al. Preparation of Bioactive Ti–Nb–Ta–Zr Alloy by Chemical Treatment. Aichi: Japanese Society of Orthopaedic Ceramic Implants; 2009.

[19] Kizuki T, Takadama H, Matsushita T, Nakamura T, Kokubo T. Preparation of bioactive Ti metal surface enriched with calcium ions by chemical treatment. Acta Biomater 2010.

[20] Fujibayashi S, Neo M, Kim HM, Kokubo T, Nakamura T. A comparative study between in vivo bone ingrowth and in vitro apatite formation on Na_2O–CaO–SiO_2 glasses. Biomaterials 2003;24:1349–56.

[21] Nakamura T, Yamamuro T, Higashi S, Kokubo T, Itoo S. A new glass-ceramic for bone replacement: evaluation of its bonding to bone tissue. J Biomed Mater Res 1985;19:685–98.

[22] Kokubo T, Takadama H. How useful is SBF in predicting in vivo bone bioactivity? Biomaterials 2006;27:2907–15.

[23] Onishi E, Fujibayashi S, Takemoto M, Neo M, Maruyama T, Kokubo T, et al. Enhancement of bone-bonding ability of bioactive titanium by prostaglandin E_2 receptor selective agonist. Biomaterials 2008;29:877–83.

[24] Maniatopoulos C, Rodriguez A, Deporter DA, Melcher AH. An improved method for preparing histological sections of metallic implants. Int J Oral Maxillofac Implants 1986;1:31–7.

[25] Takemoto M, Nakamura T. Osteoconduction and its evaluation. In: Kokubo T, editor. Bioceramics and their Clinical Applications. Cambridge: Woodhead Publishing; 2008. p. 183–98.

[26] Okazaki Y, Nishimura E, Nakada H, Kobayashi K. Surface analysis of Ti–15Zr–4Ta alloy after implantation in rat tibia. Biomaterials 2001;22:599–607.

[27] Sumitomo N, Noritake K, Hattori T, Morikawa K, Niwa S, Sato K, et al. Experiment study on fracture fixation with low rigidity titanium alloy: plate fixation of tibia fracture model in rabbit. J Mater Sci Mater Med 2008;19:1581–6.

[28] Takadama H, Kim HM, Kokubo T, Nakamura T. An X-ray photoelectron spectroscopy study of the process of apatite formation on bioactive titanium metal. J Biomed Mater Res 2001;55:185–93.

[29] Takadama H, Kim HM, Kokubo T, Nakamura T. TEM–EDX study of mechanism of bonelike apatite formation on bioactive titanium metal in simulated body fluid. J Biomed Mater Res 2001;57:441–8.

[30] Ohtsuki C, Kokubo T, Yamamuro T. Mechanism of apatite formation on CaO–SiO_2–P_2O_5 glasses in a simulated body fluid. J Non-Cryst Solids 1992;143:84–92.

[31] Chen XB, Li YC, Du Plessis J, Hodgson PD, Wen C. Influence of calcium ion deposition on apatite-inducing ability of porous titanium for biomedical applications. Acta Biomater 2009;5:1808–20.

[32] Nayab SN, Jones FH, Olsen I. Effects of calcium ion implantation on human bone cell interaction with titanium. Biomaterials 2005;26:4717–27.

[33] Park JW, Park KB, Suh JY. Effects of calcium ion incorporation on bone healing of Ti6Al4V alloy implants in rabbit tibiae. Biomaterials 2007;28:3306–13.

Preparation of bioactive Ti-15Zr-4Nb-4Ta alloy from HCl and heat treatments after an NaOH treatment

Seiji Yamaguchi,[1] Hiroaki Takadama,[1] Tomiharu Matsushita,[1] Takashi Nakamura,[2] Tadashi Kokubo[1]

[1]Department of Biomedical Sciences, College of Life and Health Sciences, Chubu University, 1200 Matsumoto-cho, Kasugai-city, Aichi 487-8501, Japan
[2]Department of Orthopaedic Surgery, Graduate School of Medicine, Kyoto University, Kawaharacho54, Shogoin, Sakyo-ku, Kyoto 606-8507, Japan

Received 4 October 2010; revised 2 December 2010; accepted 17 December 2010
Published online 2 March 2011 in Wiley Online Library (wileyonlinelibrary.com). DOI: 10.1002/jbm.a.33036

Abstract: Ti-15Zr-4Nb-4Ta alloy does not contain any cytotoxic elements and has a high mechanical strength. Water or HCl and heat treatments were applied to this alloy after NaOH treatment to form a bioactive titanium oxide layer with a nanometer scale roughness on its surface. The nanometer scale roughness was formed on the surface after the first NaOH treatment and remained, even after a subsequent water or HCl and heat treatment. A layer that was mainly composed of anatase was formed on the surface after the heat treatment. Thus, the treated alloy showed a high apatite-forming ability in an SBF, as well as a high scratch resistance. Its high apatite-forming ability was attributed to its positive surface charge. The same alloy subjected to a heat treatment without a water or HCl treatment after the NaOH treatment did not show an apatite-forming ability. This was attributed to a too slow release rate of sodium ions from the surface in an SBF. Ti-15Zr-4Nb-4Ta alloy samples subjected to a water or HCl and heat treatment after the NaOH treatment are expected to be useful as orthopedic and dental implants, since they can form an apatite layer on their surface in a living body and bond to living bone through this apatite layer. © 2011 Wiley Periodicals, Inc. J Biomed Mater Res Part A: 97A: 135–144, 2011.

Key Words: Ti-15Zr-4Nb-4Ta alloy, acid, positive charge, apatite, cytotoxic-free

INTRODUCTION

Because of their high mechanical strength and good biocompatibility, titanium (Ti) metal and its alloys are widely used in various implants, such as in artificial joints and tooth roots in orthopedic surgery and dentistry. However, they do not bond to living bone, and hence, their fixation to the surrounding bone is not stable for a long period. It has been reported that Ti metal with a surface sodium titanate layer formed after an NaOH and heat treatment forms a bonelike apatite layer on its surface in the living body, and bonds to living bone through this apatite layer.[1–4] This type of chemical and heat treatment has been applied to the porous titanium metal surface layer of an artificial total hip joint, and has been used clinically in Japan since 2007.[5]

The above treatment is effective for inducing bone-bonding bioactivity in conventional Ti-based alloys, such as Ti-6Al-4V,[6] Ti-15Mo-5Zr-3Al,[7] and Ti-6Al-2Nb-1Ta.[2] However, these treatments are not effective in inducing apatite-forming ability in the new Ti-Zr-Nb-Ta alloys,[8] which are free from elements suspected of cytotoxicity. Among these alloys, Ti-15Zr-4Nb-4Ta (Ti-15-4-4) alloy shows a high mechanical strength.[9]

We have previously shown that if this alloy is subjected to NaOH, $CaCl_2$, heat, and water treatments, it forms a Ca-deficient calcium titanate on its surface, and exhibits an apatite-forming ability in a body environment.[10] However, metals enriched with sodium or calcium ions on their surfaces tend to release the sodium or calcium ions to some degree via exchange with oxonium ions in a body fluid, increase pH of surrounding environment by consuming the oxonium ions in it, and, therefore, are liable to have an unfavorable effect on living cells, especially in the narrow spaces of a porous body.

On the other hand, recently, it has also been shown that Ti metal bonds to living bone, if it has been subjected to a heat treatment after an acid treatment to form a titanium oxide layer on its surface.[11] It should be noted that thus formed titanium oxide layer does not release any ions into surrounding fluid in body environment. However, there is a difference in the surface topography after the alkaline and acid treatments. The former treatment gives a nanometer scale roughness, whereas the latter treatment gives a micrometer scale roughness. It is assumed that a nanometer scale roughness may be more suitable for the surface of porous Ti metal in terms of its osteoconductivity as well as osteoinductivity,[12] if the layer does not release any ions. A layer of

Correspondence to: S. Yamaguchi; e-mail: sy-esi@isc.chubu.ac.jp
Contract grant sponsor: Translational Research Promotion Project in Health Assurance Program entrusted from the New Energy and Industrial Technology Development Organization (NEDO)

soluble-ion-free bioactive titanium oxide with a nanometer scale roughness may be formed on Ti metal by applying acid and heat treatments after an NaOH treatment. It has already been reported that such a surface layer is formed on Ti metal if it is subjected to an HCl and heat treatment after an NaOH treatment.[13] From animal experiments, it was confirmed that porous Ti metal subjected to the same treatment exhibits osteoconductivity[14] as well as osteoinductivity.[15]

The aim of this study is to investigate the conditions of chemical and heat treatments for producing a surface layer on Ti-15-4-4 alloy that shows high apatite-forming ability in a body environment without giving any ion release in surrounding fluid, and has a nanometer scale roughness which is considered to be effective for osteoinductivity.[15] The factor governing its high apatite-forming ability is discussed from a view point of surface potential of the Ti-15-4-4 alloy subjected to the chemical and heat treatments.

Regarding the formation of a titanium oxide layer having an apatite-forming ability on Ti-15-4-4 alloy, Sugino et al.[16] have already reported that a rutile layer forms on this alloy after a heat treatment at 500°C precipitates apatite in a simulated body fluid (SBF), but only in the internal surfaces of microgrooves. The reason for the formation of apatite is not yet known.

MATERIALS AND METHODS

Sample and surface treatments

Ti-15-4-4 alloy (Ti = balance, Zr = 14.51, Nb = 3.83, Ta = 3.94, Pd = 0.16, and O = 0.25 mass%) supplied by the Kobelco Research Institute, Inc., Japan, was cut into rectangular-shaped samples with dimensions of 10 × 10 × 1 mm^3, abraded with 400 diamond plates, and washed with acetone, 2-propanol, and ultrapure water in an ultrasonic cleaner for a period of 30 min, and then dried at 40°C. The samples were soaked in 5 mL of a 5*M* NaOH aqueous solution at 60°C for a period of 24 h in an oil bath, and then shaken at a speed of 120 strokes/min. After being removed from the solution, the alloy samples were gently rinsed with ultrapure water for a period of 30 s, and dried at 40°C. The samples were subsequently soaked in 10 mLof a dilute HCl solution at a concentration of 0.5 or 50 m*M* at 40°C for a period of 24 h. The HCl treatment using a 0.5 or 50 m*M* HCl solution is denoted in the manuscript as a 0.5 HCl or 50 HCl treatment, respectively. For reference, the alloy sample was soaked in 200 mL of ultrapure water at 40°C for a period of 24 h after the NaOH treatment, where the ultrapure water was refreshed after a period of 12 h. The alloy samples were then removed from the solution, washed with ultrapure water, and then dried. After the chemical treatment, they were heated to 600°C at a rate of 5°C/min in a Fe-Cr electrical furnace in air, kept at 600°C for a period of 1 h, and then allowed to cool at the natural rate of the furnace.

Soaking in an SBF

The samples subjected to chemical and heat treatments were soaked at 36.5°C in 24 mL of a simulated body fluid (SBF)[17] having ion concentrations nearly equal to those of human blood plasma (Na^+ = 142.0, K^+ = 5.0, Ca^{2+} = 2.5, Mg^{2+} = 1.5, Cl^- = 147.8, HCO_3^- = 4.2, HPO_4^{2-} = 1.0, and SO_4^{2-} = 0.5 m*M*). The SBF was prepared by dissolving reagent-grade NaCl, $NaHCO_3$, KCl, $K_2HPO_4{\cdot}3H_2O$, $MgCl{\cdot}6H_2O$, $CaCl_2$, and Na_2SO_4 (Nacalai Tesque, Inc., Kyoto, Japan) in ultrapure water and buffed at pH = 7.4 with tris hydroxymethylaminomethane $(CH_2OH)_3CNH_2$ (Nacalai Tesque, Inc., Kyoto, Japan), and 1*M* HCl at 36.5°C. After soaking in the SBF for 3 d, the samples were removed from the SBF, gently rinsed with ultrapure water and dried at 40°C.

Surface analysis

Scanning electron microscopy. The surface and cross-sectional area of the alloy samples subjected to chemical and heat treatments, and those subsequently soaked in an SBF were coated with a Pt/Pd film and observed under a field-emission scanning electron microscope (FE-SEM; S-4300, Hitachi Co., Japan) using an acceleration voltage of 15 kV. The sample preparation for the cross-sectional observations followed the procedure given in our previous article.[18]

Thin film X-ray diffraction and Fourier-transform confocal laser Raman spectroscopy. The surface of the alloy samples subjected to the chemical and heat treatments, and those subsequently soaked in an SBF were analyzed using thin film X-ray diffraction (TF-XRD, Model RNT-2500, Rigaku Co., Japan) and Fourier transform confocal laser Raman spectroscopy (FT-Raman, LabRAM HR800, Horiba Jobin-Yvon, France). The TF-XRD used a CuKα X-ray source operating at 50 kV and 200 mA, and the glancing angle of the incident beam was set to an angle of 1° against the sample surface. The FT-Raman used an argon laser with a wavelength of 514.5 nm as the laser source.

Scratch resistance measurements. The scratch resistance of the surface layer formed on the alloy samples from the chemical and heat treatments was measured using a thin film scratch tester (Model CSR-2000, Rhesca Co., Japan), employing a stylus with a diameter of 5 μm with a spring constant of 200 g/mm. Based on the data in the JIS R-3255 standard, the amplitude, scratch speed, and loading rate used were 100 μm, 10 μm/s, and 100 mN/min, respectively. Five measurements were carried out for each sample, and the average value was used in our analysis.

Zeta potential measurements. Large size Ti-15-4-4 plates (dimensions = 13 × 33 × 1 mm^3) were prepared for the zeta potential measurements using the method of chemical and heat treatments described in Sample and surface treatments, where only the volumes of the solutions were increased to 15 mL for the NaOH solution, 600 mL for water, and to 30 mL of the 0.5 HCl or 50 HCl solutions, in accordance with the increase in surface area of the samples. The treated alloy samples were electrically grounded to allow for any leakage of stray charge, and were immediately set in a zeta potential and particle size analyzer (Model ELS-Z1, Otsuka Electronics Co., Japan) using a glass cell for the plate sample. The zeta potential of the samples was

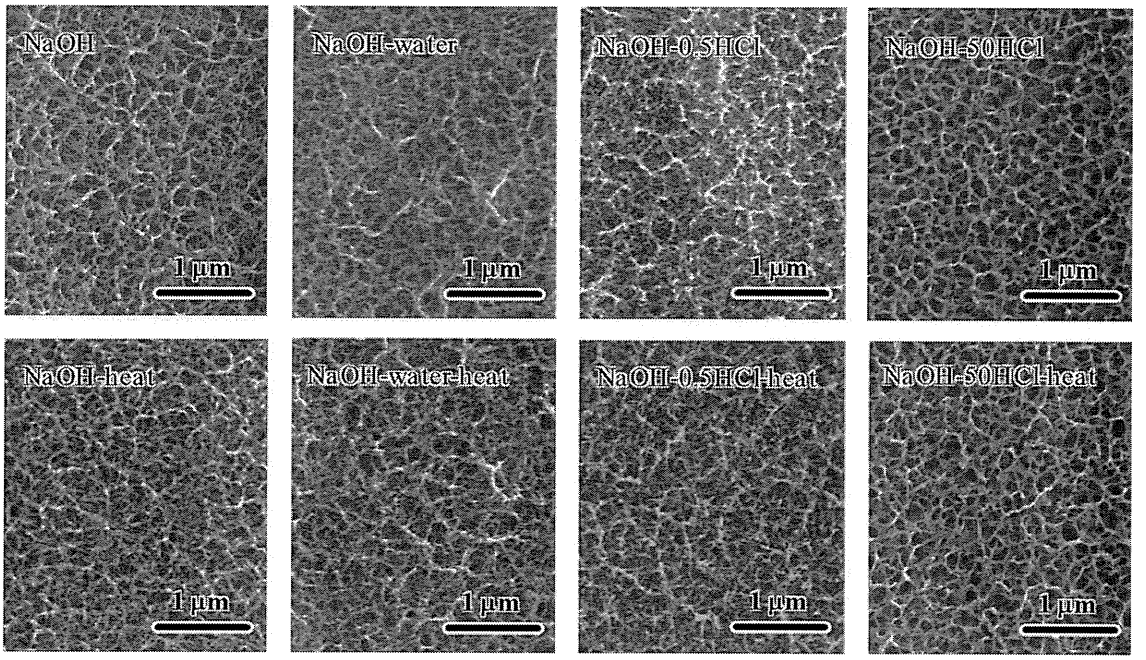

FIGURE 1. FE-SEM photographs of the surfaces of NaOH-treated Ti-15Zr-4Nb-4Ta alloy subsequently subjected to water, 0.5 HCl, or 50 HCl, and heat treatments.

measured under an applied voltage of 40 V in a 50 or 100 m*M* NaCl solution. The dispersant monitoring particles of polystyrene latex (size = 500 nm) were coated with hydroxyl propyl cellulose. Five samples were measured for each experimental condition, and the average value was used in our analysis.

X-ray photoelectron spectroscopy. The surfaces of the alloy samples soaked in the SBF for various periods after the chemical and heat treatments were analyzed using X-ray photoelectron spectroscopy (XPS, ESCA-3300KM, Shimadzu Co., Japan). In our analysis, Mg-Kα radiation ($\lambda = 9.8903$ Å) was used as the X-ray source. The XPS take-off angle was set at 45 degrees, which enabled the system to detect photoelectrons to a depth of 5 to 10 nm from the surface. The binding energy of the measured spectra was calibrated by reference to the C_{1s} peak of the surfactant CH_2 groups on the substrate at 284.6 eV. The measured spectra were decomposed and subjected to curve fitting for quantitative analysis.

RESULTS

Surface structure

Figure 1 shows FE-SEM photographs of the surface of the alloy samples subjected to water, 0.5 HCl or 50 HCl, and heat treatments after an NaOH treatment. A fine network structure on the nanometer scale was formed on the surface of the alloy after the initial NaOH treatment, and this was essentially unchanged by the subsequent chemical and heat treatments.

Figure 2 shows FE-SEM photographs of the cross-section of the samples shown in Figure 1. A 500-nm thick layer, which was composed of many feather-like phases that were elongated perpendicular to the surface, had formed on the surface of the Ti-15-4-4 alloy after the NaOH treatment. The density of the surface layer increased with increasing depth. The thickness of the surface layer was unchanged by the subsequent water or 0.5 HCl treatment, but decreased slightly after the 50 HCl treatment. The subsequent heat treatment did not change the surface structure.

Table I shows the result of the XPS quantitative analysis of the surface of the alloy samples subjected to the NaOH, water, 0.5 HCl, or 50 HCl, and heat treatments. The NaOH treatment incorporated 4.9 atm. % of Na ions into the surface of the alloy samples. The Na ions were completely removed by both the subsequent water and 0.5 HCl or 50 HCl treatment. It should be noted that some of the alloying elements, such as Zr, Nb, and Ta were released by the NaOH treatment, but some remained, even after the subsequent water and 0.5 HCl or 50 HCl treatment. The slight increase in minor alloying elements after the 50HCl treatment reflected the decrease in thickness of the surface layer. When the NaOH-treated sample was heated, the Na content significantly increased to 12.3 atm. %, indicating that the surface layer was densified after the heat treatment after dehydration. The heat treatment induced no apparent changes in the chemical composition for the NaOH-water- and NaOH-0.5 HCl-treated samples, but a slight increase in the Zr, Nb, and Ta contents was detected for the NaOH-50 HCl-treated sample.

Figure 3 shows the TF-XRD and FT-Raman profiles of the surface of the alloy samples subjected to the NaOH, and then a water and 0.5 HCl or 50 HCl treatment. The broad TF-XRD peaks occurring around $2\theta = 24$, 28, and 48

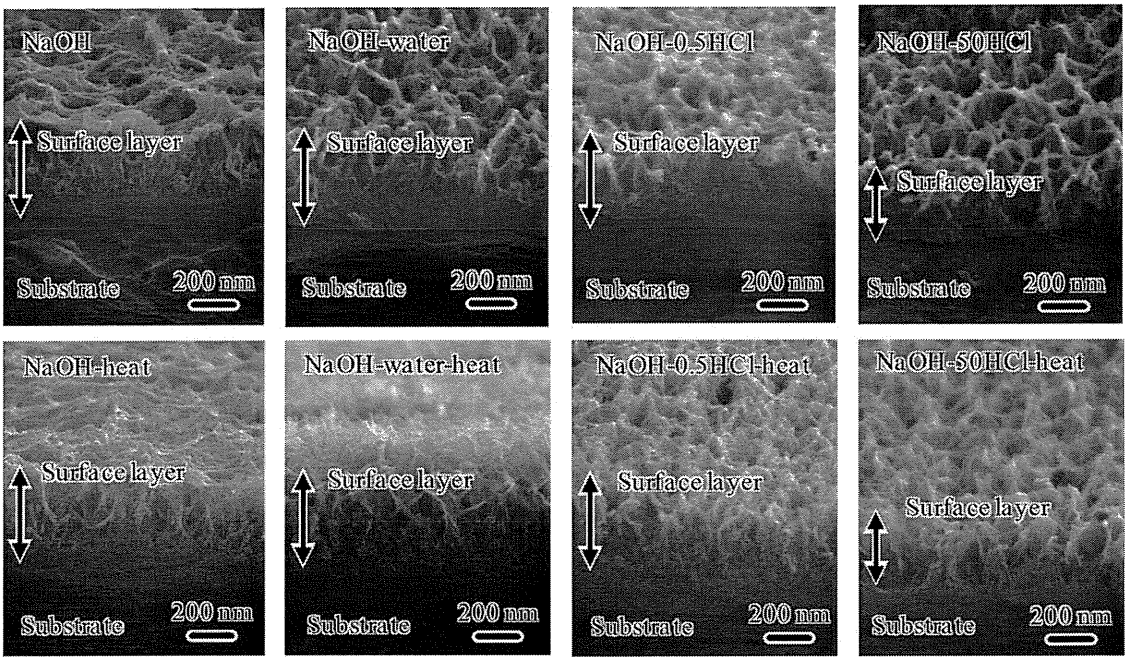

FIGURE 2. FE-SEM micrographs of the cross-sections of NaOH-treated Ti-15Zr-4Nb-4Ta alloy subsequently subjected to water, 0.5 HCl, or 50 HCl, and heat treatments.

degrees and FT-Raman peaks occurring around wavenumbers = 280, 450, 700, 820, and 910 cm^{-1} after the NaOH treatment were assigned to sodium hydrogen titanate ($Na_xH_{2-x}Ti_3O_7$).[19,20] When the NaOH-treated samples were subjected to water and 0.5 HCl or 50 HCl treatments, the intensity of the TF-XRD peak occurring around 2θ = 28 degrees and the Raman peak occurring around wave number = 910 cm^{-1} decreased, indicating that the sodium hydrogen titanate had transformed into hydrogen titanate ($H_2Ti_3O_7$)[19,20] as a result of the exchange of the sodium and oxonium ions.

Figure 4 shows the TF-XRD and FT-Raman profiles of the alloy samples that were subsequently subjected to a heat treatment. When the NaOH-treated sample was subsequently heat treated, the sodium hydrogen titanate layer transformed into sodium titanate ($Na_2Ti_6O_{13}$) accompanied with anatase and rutile phases. On the other hand, when the NaOH-, and the water- and 0.5 HCl- or 50 HCl-treated samples were heat treated, the hydrogen titanate layer was converted to anatase, accompanied by a small amount of rutile.

Figure 5 shows the scratch resistance of the surface of the alloy samples subjected to NaOH, water, 0.5 HCl or 50 HCl, and heat treatments. The scratch resistance of the NaOH-treated sample was as low as 10 m*N*, and was not changed by either a subsequent water or 0.5 HCl or 50 HCl treatment. However, the scratch resistance increased significantly to >90 m*N* after a subsequent heat treatment.

The zeta potential was not able to be measured for the alloy samples subjected to the NaOH, and water and 0.5 HCl or 50 HCl treatments, since their surface was electrically conducting. Figure 6 shows the zeta potential of alloy samples subjected to a heat treatment after an NaOH, and subsequent water and 0.5 HCl or 50 HCl treatment. The alloy samples heat treated after the NaOH treatment showed a negative zeta potential, around −7 mV, whereas samples of

TABLE I. Result of XPS Quantitative Analysis of Surface Layer of Ti-15Zr-4Nb-4Ta Alloy Untreated and Subjected to NaOH, water, 0.5 HCl, or 50 HCl, and Heat Treatments

	Element/atm. %						
Treatment	O	Ti	Na	Zr	Nb	Ta	Pd
Untreated	73.7	21.2	0	3.7	0.9	0.6	0
NaOH	69.6	23.9	4.9	1.1	0.4	0.2	0
NaOH–water	72.1	26.0	0	1.0	0.6	0.4	0
NaOH–0.5 HCl	72.0	26.2	0	0.9	0.6	0.4	0
NaOH–50 HCl	72.9	23.8	0	1.6	1.2	0.4	0
NaOH–heat	63.6	22.4	12.3	0.8	0.8	0.2	0
NaOH–water-heat	72.0	25.3	0	1.1	1.2	0.4	0
NaOH–0.5 HCl-heat	72.0	25.8	0	1.0	0.8	0.4	0
NaOH–50 HCl-heat	72.9	22.3	0	2.3	1.9	0.7	0

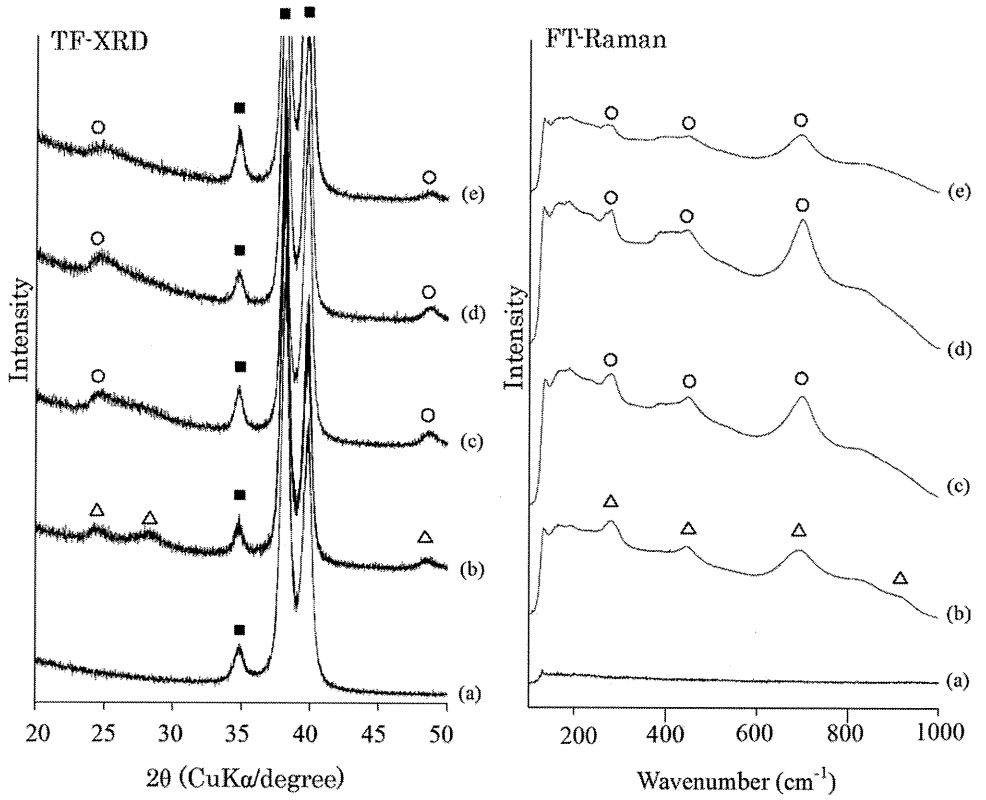

FIGURE 3. TF-XRD and FT-Raman profiles of the surfaces of Ti-15Zr4Nb-4Ta- alloy (a) untreated and subjected to (b) NaOH treatment, (c) NaOH and water treatments, (d) NaOH and 0.5 HCl treatments, and (e) NaOH and 50 HCl treatments. ■, α-Titanium; △, sodium hydrogen titanate ($Na_xH_{2-x}Ti_3O_7$); ○, hydrogen titanate ($Na_xH_{2-x}Ti_3O_7$).

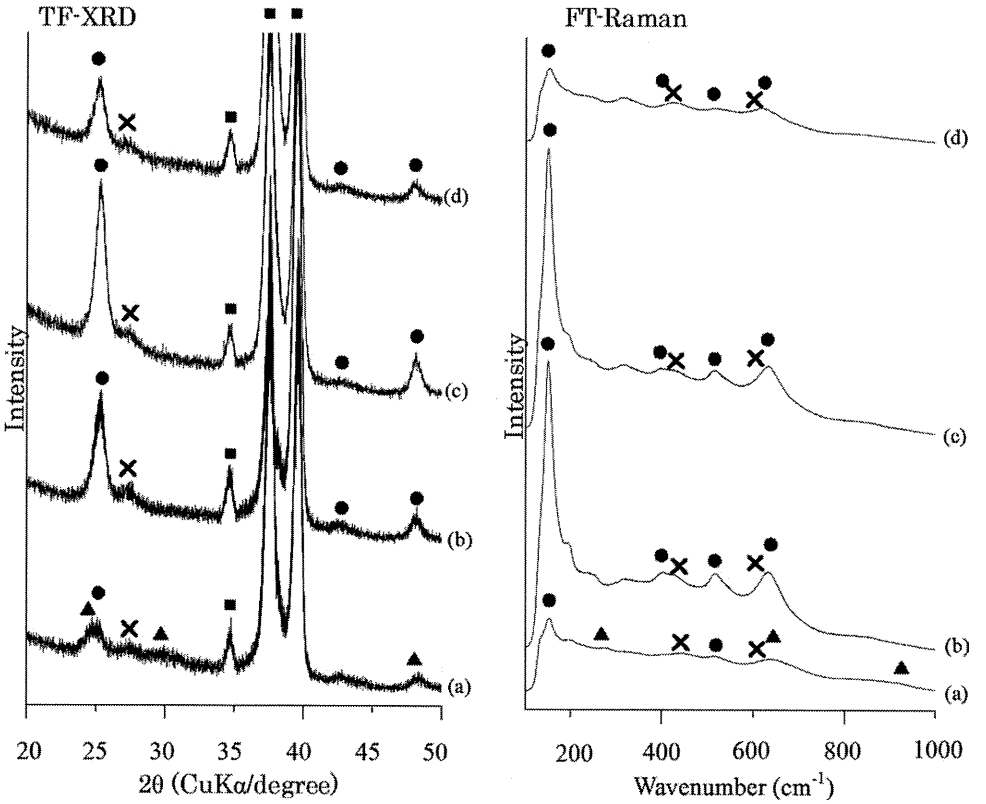

FIGURE 4. TF-XRD and FT-Raman profiles of the surfaces of Ti-15Zr-4Nb-4Ta alloy subjected to (a) NaOH and heat treatments, (b) NaOH, water, and heat treatments, (c) NaOH, 0.5 HCl, and heat treatments, and (d) NaOH, 50 HCl, and heat treatments. ■, α-Titanium; ▲, sodium titanate ($Na_2Ti_6O_{13}$); ●, Anatase; ×, Rutile.

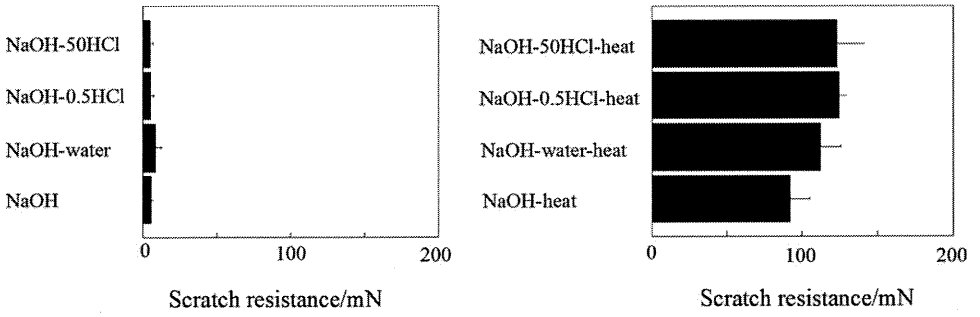

FIGURE 5. Scratch resistance of NaOH-treated Ti-15Zr-4Nb-4Ta alloy subsequently subjected to water, 0.5 HCl, or 50 HCl, and heat treatments.

the same alloy heat treated after a water and 0.5 HCl or 50 HCl treatment following the NaOH treatment showed a positive zeta potential, around +3 mV.

Apatite-forming ability in an SBF

Figure 7 shows FE-SEM photographs of the surface of alloy samples that were soaked in an SBF for 3 d after an NaOH, and water and 0.5 HCl or 50 HCl treatment, and then a heat treatment. Spherical precipitates, identified as crystalline apatite from the TF-XRD data, had formed on the surface of the NaOH-treated sample. However, these apatite particles disappeared after the subsequent heat treatment. The NaOH-treated samples subjected to a water and 0.5 HCl or 50 HCl treatment did not show the formation of apatite on their surface. However, they formed apatite extensively on their surface when they were subsequently heat treated.

Figure 8 shows the Ca 2s and P 2p XPS profiles measured from the surfaces of alloy samples soaked in an SBF after an NaOH and heat or NaOH and 50 HCl and a heat treatment as a function of the soaking time in the SBF. As can be seen from Figure 8, the alloy samples heat treated after the NaOH treatment had initially adsorbed calcium ions selectively on their surface, and then phosphate ions, whereas those samples that were heat treated after the 50 HCl treatment following an NaOH treatment had initially adsorbed phosphate ions selectively on their surface, followed by calcium ions.

DISCUSSION

It can be seen from Figure 1 that a nanometer scale roughness was produced on the surface of Ti-15-4-4 alloy by the NaOH treatment, and that this remained, even after subsequent HCl and heat treatments, as in the case of pure Ti metal.[20] The nanometer scale roughness had a brush-like structure consisting of feather-like phases elongated perpendicular to the surface to a thickness of about 500 nm (see Fig. 2). The feather-like phases consisted of nano-sized sodium hydrogen titanate ($Na_xH_{2-x}Ti_3O_7$) after the NaOH treatment. The sodium hydrogen titanate was transformed into sodium titanate ($Na_2Ti_6O_{13}$) and anatase when the alloy was immediately subjected to a heat treatment (see Figs. 3 and 4), whereas the sodium hydrogen titanate was transformed into hydrogen titanate ($H_2Ti_3O_7$) when it was soaked in water and 0.5 HCl or 50 HCl solution, and then transformed into anatase accompanied by a small amount of rutile after a subsequent heat treatment (see Figs. 3 and 4), as shown schematically in Figure 9.

The scratch resistance of the surface layer increased markedly after the heat treatment in both cases. However, the apatite-forming ability in an SBF of the alloy decreased after the heat treatment in the former case, whereas it increased markedly in the latter case. In the case of Ti metal, an apatite-forming ability of an NaOH-treated metal is increased after a subsequent heat treatment.[20] The results of the Ti-15-4-4 alloy are in contrast with those of Ti metal. These differences can be interpreted as follows. The Ti-15-4-4 alloy forms sodium titanate on its surface after the NaOH and heat treatments, as in the case of Ti metal. This sodium titanate is speculated to release sodium ions into the SBF via exchange with the oxonium ions present to form Ti-OH groups on its surface.[21,22] The Ti-OH groups formed may be negatively charged because the pH of the surrounding SBF is increased from the sodium ions released.[23] The Ti-OH groups would tend to combine with the positively charged calcium ions, and then with the phosphate ions to form apatite, as is the case for NaOH- and heat-treated Ti metal.[21,22] It was confirmed from the zeta potential data shown in Figure 6 that the Ti-15-4-4 alloy has a negatively charged surface in an NaCl solution. The sequential adsorption of the calcium and phosphate ions on the Ti-15-4-4 alloy in an SBF was confirmed by the XPS spectra shown in Figure 8.

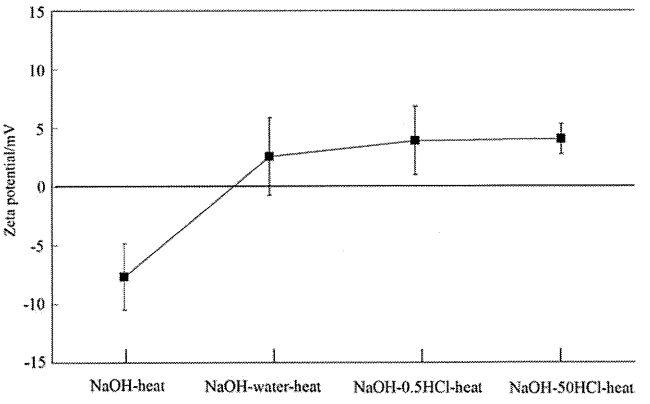

FIGURE 6. Zeta potential of NaOH-treated Ti-15Zr-4Nb-4Ta alloy subsequently subjected to water, 0.5 HCl, or 50 HCl, and heat treatments.

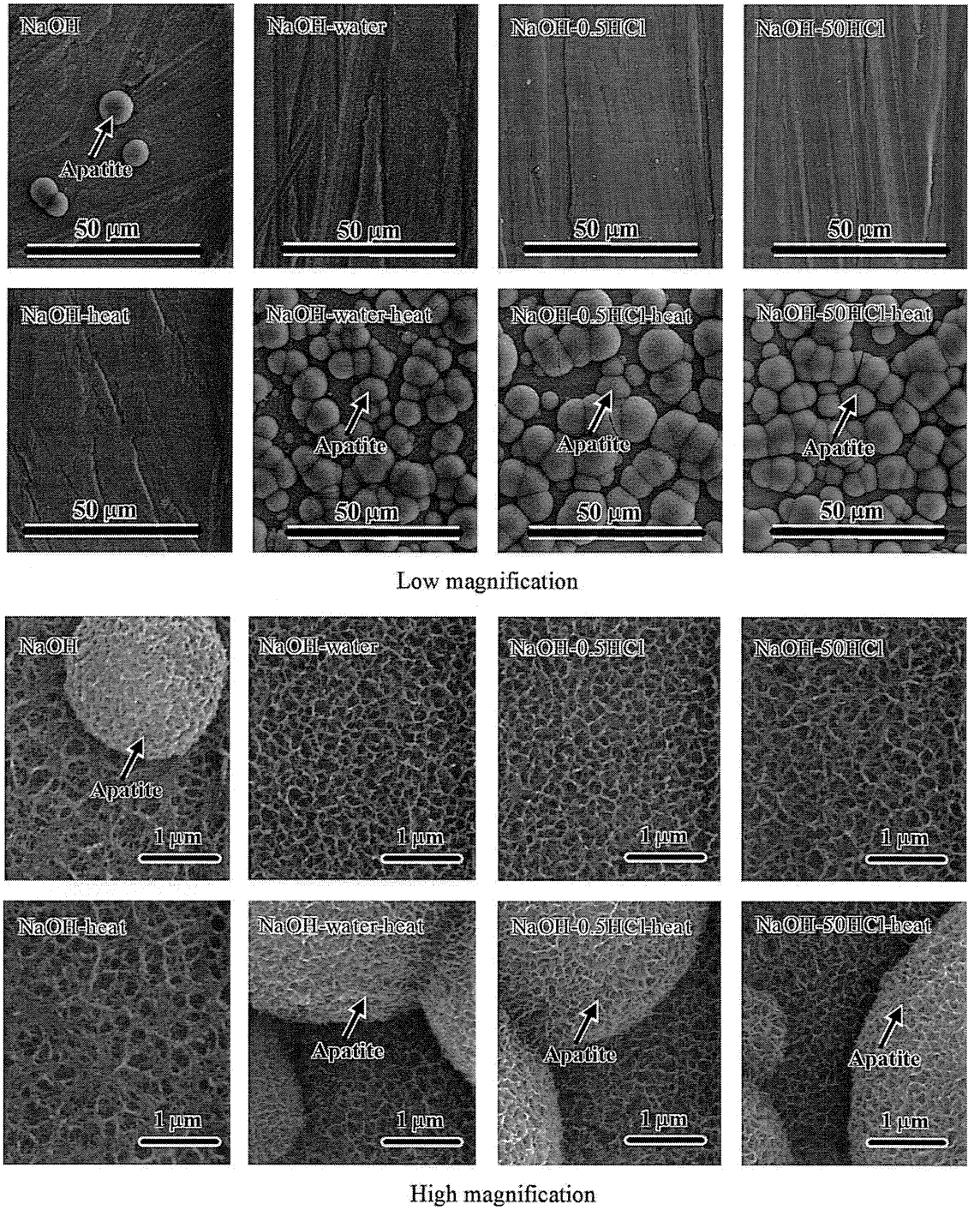

FIGURE 7. FE-SEM photographs of the surfaces of Ti-15Zr-4Nb-4Ta alloy that were soaked in SBF for 3 d after NaOH and water, 0.5 HCl, or 50 HCl, and heat treatments.

However, the thickness of the surface layer that was mainly composed of sodium titanate on the Ti-15-4-4 alloy was half that formed on Ti metal.[18] This means that the amount of sodium ions able to be released from the Ti-15-4-4 alloy was lower than that from Ti metal. In addition, the surface layer of the Ti-15-4-4 alloy contained a considerable amount of alloying elements, such as Zr, Nb, and Ta. These alloying elements can inhibit the release of sodium ions from the Ti-15-4-4 alloy. It was confirmed by measuring the release of sodium ions from the Ti-15-4-4 alloy into water that the amount and rate of sodium-ion release are low. Plate samples of the Ti-15-4-4 alloy and pure Ti metal with dimensions of $10 \times 10 \times 1$ mm^3, which were subjected to NaOH and heat treatments were soaked in 2 mL of

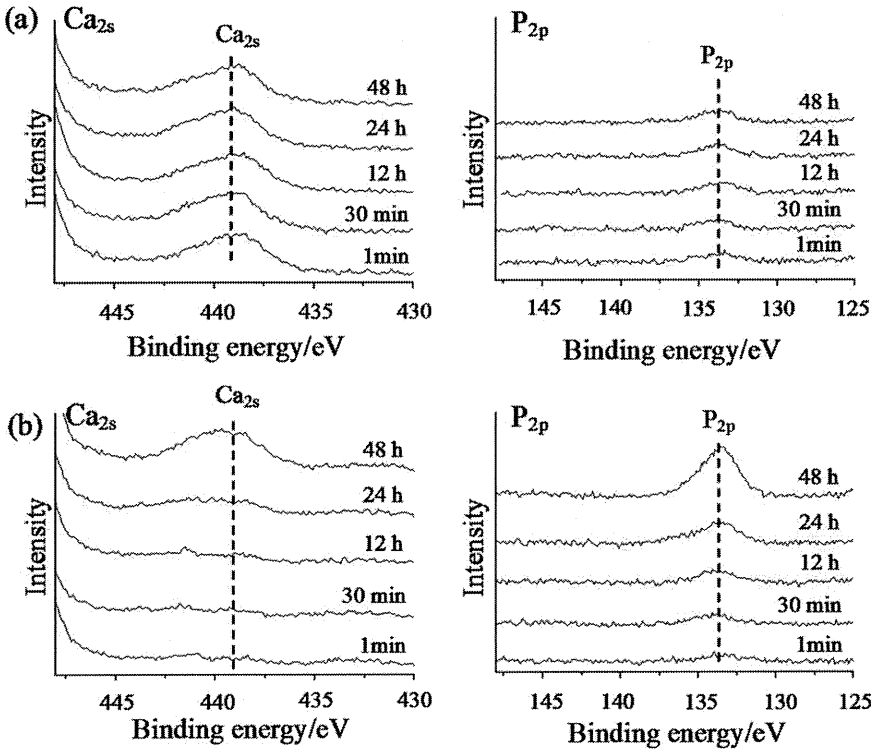

FIGURE 8. XPS profiles of the surfaces of Ti-15Zr-4Nb-4Ta alloy soaked in SBF after (a) NaOH and heat, or (b) NaOH, 50 HCl, and heat treatments as a function of soaking time in SBF.

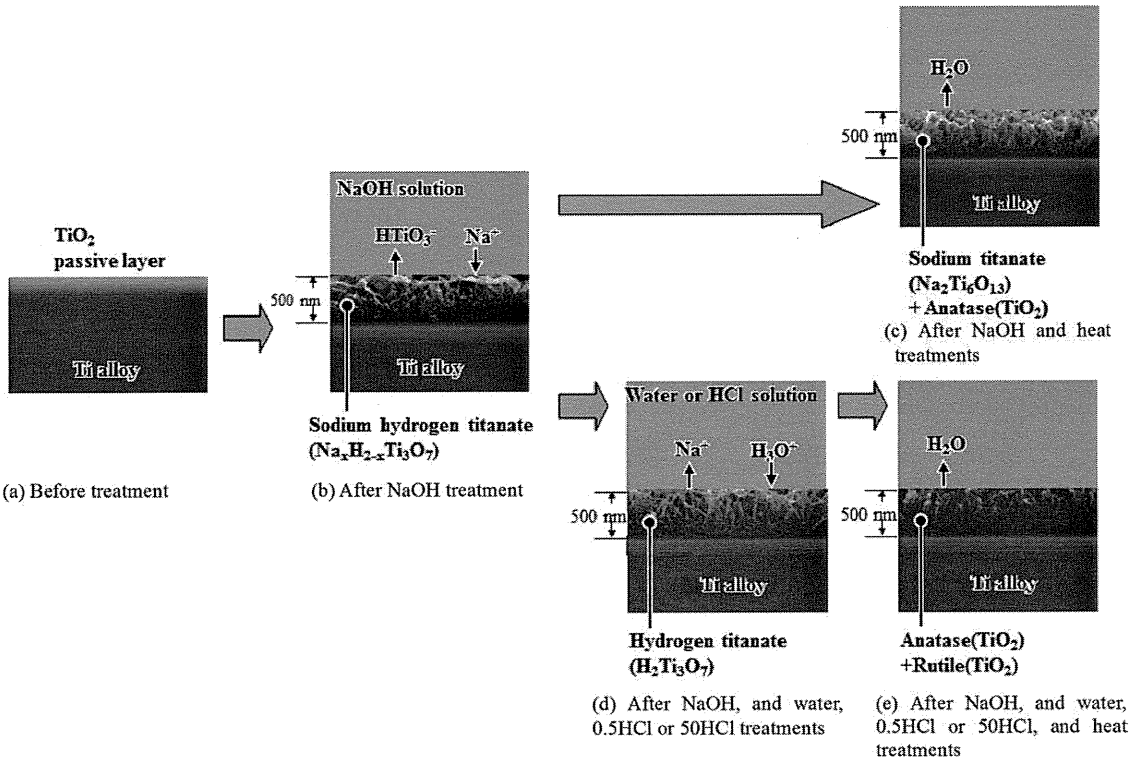

FIGURE 9. Schematic illustration of structural changes on the surface of Ti-15Zr-4Nb-4Ta alloy (a) by NaOH (b), and subsequent heat (c) treatments, or water, 0.5 HCl, or 50 HCl (d) and then heat (e) treatments.

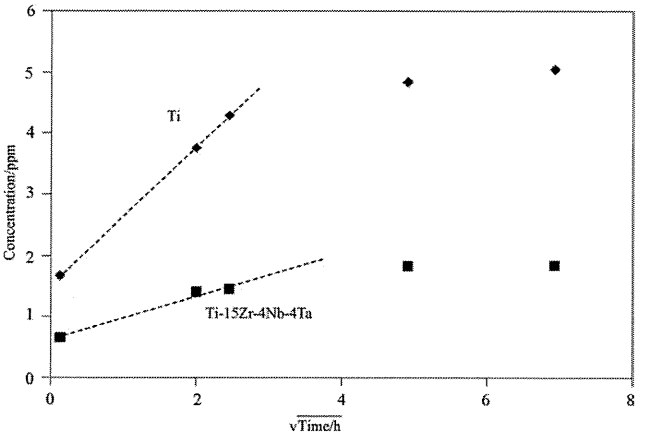

FIGURE 10. Release of sodium ions from Ti-15Zr-4Nb-4Ta alloy and Ti metal subjected to NaOH and heat treatments as a function of square root of soaking time in water, measured by ICP.

ultrapure water at 36.5°C, and the concentration of sodium ions released was measured using inductively coupled plasma (ICP, Model SPS3100, Seiko Instruments Inc., Japan) as a function of soaking time. The results shown in Figure 10 were obtained, and it can be seen that the amount and rate of release of the sodium ions from the Ti-15-4-4 alloy were markedly lower than those from pure Ti metal.

In contrast with the case of a heat treatment immediately after the NaOH treatment, the Ti-15-4-4 alloy showed a high apatite-forming ability in an SBF when it was heat treated after a water or HCl treatment following the NaOH treatment. The high apatite-forming ability of the Ti-15-4-4 alloys subjected to a water or HCl and heat treatment after the NaOH treatment can be interpreted in terms of the surface charge. As show in Figure 6, the surfaces of the Ti-15-4-4 alloy have positive charge after the water or HCl and heat treatments following the NaOH treatment. When the alloy has a positive charge on its surface, it combines selectively with negatively charged phosphate ions. As the phosphate ions begin to accumulate, its surface becomes negatively charged and combines with the positively charged calcium ions to form apatite. Such a sequential adsorption was confirmed by the XPS spectra shown in Figure 8.

The positive surface charge of the alloys subjected to HCl and heat treatments after the NaOH treatment may be attributed to the presence of chloride ions adsorbed on the surface, as in the case of Ti metal.[11] These chloride ions are adsorbed on the surface of the alloy during the HCl treatment after the NaOH treatment. These remain after the subsequent heat treatment and dissociate in the SBF to give an acidic environment on the surface of the alloy.[11] Titanium oxide is positively charged in an acid environment.[23]

In the case of Ti metal, the positive surface charge and the apatite-forming ability are increased with increasing concentration of the HCl solution,[13] because a higher concentration of chloride ions can be adsorbed on the surface in a concentrated HCl solution. However, the alloy treated with 50 HCl solution showed almost the same zeta potential and apatite-forming ability as the sample treated with the 0.5 HCl solution (see Figs. 6 and 7). This is interpreted in terms of the increased amount of alloying elements, such as Zr and Nb, after the 50HCl treatment (see Table I). It has been reported that the typical isoelectric points (IEPs) of ZrO_2 and Nb_2O_5 are around 6.5[24] and 4.1.[25] This means that both zirconium oxide and niobium oxide tend to be negatively charged at pH =7.4 in an SBF, and hence, the increase in Zr and Nb content can decrease the surface charge of the Ti-15-4-4 alloy subjected to a 50 HCl treatment.

On the other hand, the positive surface charge of the alloy subjected to water and heat treatments after the NaOH treatment cannot be interpreted in terms of the presence of chloride ions adsorbed on the alloy. It has been reported that anatase is the main phase on the surface layer of Ti-15-4-4 alloys subjected to a water and heat treatment after an NaOH treatment, and that this is slightly negatively charged in a neutral aqueous solution because its IEP value is around 6.[26] However, this value changes to within the range 4.0 to 8.3 in the presence of a small amount of impurities, or changes in the synthesis method.[27] As shown in Table I, the surface layer formed on the alloy after a water and heat treatment following the NaOH treatment contained some Zr, Nb, and Ta besides Ti and O. These elements can be incorporated into the anatase and give a positive surface charge in an SBF. It has also been reported that the surface charge of the anatase changes with crystallographic plane orientation. The (101) plane has a negative surface charge,[28] while the (001) plane has a positive surface charge.[29] Therefore, the positive surface charge on the alloy subjected to a water and heat treatment after the NaOH treatment may be interpreted in terms of the presence of impurities and/or preferred orientation of a specific crystallographic plane of the anatase.

It is apparent from our results and discussion that water or HCl and a heat treatment after the NaOH treatment forms a titanium oxide surface layer that has a nanometer scale roughness and a high apatite-forming ability on a Ti-15-4-4 alloy. Their high apatite-forming ability is attributed to their positive surface charge. Such treated porous Ti-15-4-4 alloys are expected to exhibit osteoconductivity as well as osteoinductivity, and hence, will be useful in implants in the orthopedic and dental fields. These biological properties will be examined by animal experiments in future.

CONCLUSIONS

Water or HCl and heat treatments were applied to Ti-15Zr-4Nb-4Ta alloys after an NaOH treatment. A nanometer scale roughness was produced on the surface of the alloys by the NaOH treatment, and this remained, even after a subsequent water or HCl and heat treatment. These treatments formed a titanium oxide layer that was mainly composed of anatase on the surface of the alloys. This showed a high apatite-forming ability in an SBF, as well as a high scratch resistance. The high apatite-forming ability was interpreted in terms of the positive surface charge. In contrast with this, Ti-15Zr-4Nb-4Ta alloys subjected to a heat treatment without a water or HCl treatment after the NaOH treatment did

not form apatite in an SBF. This was attributed to slow rate of release of the sodium ions from the alloy in the SBF. It is expected that such treated Ti-15Zr-4Nb-4Ta alloys subjected to a water or HCl treatment after an NaOH treatment will form an apatite layer on their surface in a living body, and will tightly bond to living bone through this apatite layer. Therefore, they will be useful as orthopedic and dental implants.

ACKNOWLEDGMENTS

The authors thank Dr. Yoshimitsu Okazaki for the supply of the alloy.

REFERENCES

1. Kokubo T, Miyaji F, Kim HM, Nakamura T. Spontaneous formation of bone-like apatite layer on chemically treated titanium metal. J Am Ceram Soc 1996;79:1127–1129.
2. Kokubo T, Miyaji F, Kim HM, Nakamura T. Preparation of bioactive Ti and its alloy via simple chemical surface treatment. J Biomed Mater Res 1996;32:409–417.
3. Yan QW, Nakamura T, Kobayashi M, Kim HM, Kokubo T. Bonding of chemically treated titanium implants to bone. J Biomed Mater Res 1997;37:267–275.
4. Nishiguchi S, Fujibayashi S, Kim HM, Kokubo T, Nakamura T. Biology of alkali- and heat- treated titanium implants. J Biomed Mater Res A 2003;67:26–35.
5. Kawanabe K, Ise K, Goto K, Akiyama H, Nakamura T, Kaneuji A, Sugimori T, Mtsumoto T. Clinical device-related article a new cementless total hip arthroplasty with bioactive titanium porous-coating by alkaline and heat treatment: Average 4.8-year results. J Biomed Mater Res B Appl Biomater 2009;90:476–481.
6. Kim HM, Takadama H, Miyaji F, Kokubo T, Nishiguchi S, Nakamura T. Formation of bioactive functionally graded structure on Ti-6Al-4V alloy by chemical surface treatment. J Mater Sci Mater Med 2000;11:555–559.
7. Kim HM, Takadama H, Kokubo T, Nishiguchi S, Nakamura T. Formation of a bioactive graded surface structure on Ti-15Mo-5Zr-3Al alloy by chemical treatment. Biomaterials 2000;21:353–358.
8. Geetha M, Singh AK, Asokamani R, Gogia AK. Ti based biomaterials, the ultimate choice for orthopedic implants—A review. Prog Mater Sci 2009;54:397–425.
9. Okazaki Y, Rao S, Ito Y, Tateishi T. Corrosion resistance, mechanical properties, corrosion fatigue strength and cytocompatibility of new Ti alloys without Al and V. Biomaterials 1998;19:1197–1215.
10. Yamaguchi S, Takadama H, Matsushita T, Nakamura T, Kokubo T. Apatite-forming ability of Ti-15Zr-4Nb-4Ta alloy induced by calcium solution treatment. J Mater Sci Mater Med 2010;21:439–444.
11. Kokubo T, Pattanayak DK, Yamaguchi S, Takadama H, Matsushita M, Kawai T, Takemoto M, Fujibayashi S, Nakamura T. Positively charged bioactive Ti metal prepared by simple chemical and heat treatments. J R Soc Interface 2010;7:S503–S513.
12. de Brujin JD, Shankar K, Yuan H, Habibovic P. Osteoinduction and its evaluation. In: Kokubo T, editor, Bioceramics and their Clinical Applications. Cambridge: Woodhead; 2008. p 199–219.
13. Pattanayak DK, Kawai T, Matsushita T, Takadama H, Nakamura T, Kokubo T. Effect of HCl concentrations on apatite-forming ability of NaOH-HCl-heat-treated titanium metal. J Mater Sci Mater Med 2009;20:2401–2411.
14. Fujibayashi S, Nakamura T, Nishiguchi S, Tamura J, Uchida M, Kim HM, Kokubo T. Bioactive titanium: Effect of sodium removal on the bone-bonding ability of bioactive titanium prepared by alkali and heat treatment. J Biomed Mater Res 2001;56: 562–570.
15. Takemoto M, Fujibayashi S, Neo M, Suzuki J, Matsushita T, Kokubo T, Nakamura T. Osteoinductive porous titanium implants: Effect of sodium removal by dilute HCl treatment, Biomaterials 2006;27:2682–2691.
16. Sugino A, Ohtsuki C, Tsuru K, Hayakawa S, Nakano T, Okazaki Y, Osaka A. Effect of spatial design and thermal oxidation on apatite formation on Ti-15Zr-4Ta-4Nb alloy, Acta Biomater 2009;5: 298–304.
17. Kokubo T, Takadama H. How useful is SBF in predicting in vivo bone bioactivity? Biomaterials 2006;27:2907–2915.
18. Yamaguchi S, Takadama T, Matsushita T, Nakamura T, Kokubo T. Cross-sectional analysis of the surface ceramic layer developed on Ti metal by NaOH-heat treatment and soaking in SBF. J Ceram Soc Japan 2009;117:1126–1130.
19. Sun X, Li Y. Synthesis and characterization of ion-exchangeable titanate nanotubes. Chem Eur J 2003;9:2229–2238.
20. Kawai T, Kizuki T, Takadama H, Matsushita T, Kokubo T, Unuma H, Nakamura T. Apatite formation on surface titanate layer with different Na content on Ti metal. J Ceram Soc Japan 2010;9:19–24.
21. Kim HM, Himeno T, Kawashita M, Lee JH, Kokubo T, Nakamura T. Surface potential change in bioactive titanium metal during the process of apatite formation in simulated body fluid. J Biomed Mater Res A 2003;67:1305–1309.
22. Takadama H, Kim HM, Kokubo T, Nakamura T. TEM-EDX Study of mechanism of bonelike apatite formation on bioactive titanium metal in simulated body fluid. J Biomed Mater Res 2001;57:441–448.
23. Textor M, Sitting C, Franchiger V, Tosatti S, Brunette DM. Properties and biological significance of natural oxide films on titanium and its alloys. In: Brunette DM, Tengrall P, Textor M, Thomsen P, editors. Tianium in Medicine. Verlag: Springer; 2001. p172–230.
24. Hook MS, Hartley PG, Thistlethwaite PJ. Fabrication and characterization of spherical zirconia particles for direct force measurement using the atomic force microscope. Langmuir 1999;15: 6220–6225.
25. Kosmulski M. Attempt to determine pristine points of zero charge of Nb_2O_5, Ta_2O_5, and HfO_2. Langmuir 1997;13:6315–6320.
26. Kiyono M. Sanka titan-bussei to ouyougijutsu. Japan: Gihodo; 1991.
27. Kosmulski M. Surface Charging and Points of Zero Charge. US: CRC press; 2009.
28. Barnard AS, Zapol P, Curtiss LA. Modeling the morphology and phase stability of TiO_2 nanocrystals in water. J Chem Theory Comput 2005;1:107–116.
29. Blomquist J, Walle IF, Uvdal P, Borg A, Sandell A. Water dissociation on single crystalline anatase TiO_2(001) studied by photoelectron spectroscopy. J Phys Chem C Nanomater Interfaces 2008; 112:16616–16621.

The long-term in vivo behavior of polymethyl methacrylate bone cement in total hip arthroplasty

Hiroyuki Oonishi[1*], Haruhiko Akiyama[2*], Mitsuru Takemoto[2], Toshiyuki Kawai[2], Koji Yamamoto[2], Takao Yamamuro[3], Hironobu Oonishi[1], and Takashi Nakamura[2]

* These authors contributed equally to this work.

[1]H. Oonishi Memorial Joint Replacement Institute, Tominaga Hospital, Osaka; [2] Department of Orthopaedics, Kyoto University, Kyoto; [3]Research Institute for Production Development, Kyoto, Japan
Correspondence: hakiyama@kuhp.kyoto-u.ac.jp
Submitted 11-02-01. Accepted 11-06-28

Background and purpose The long-term success of cemented total hip arthroplasty (THA) has been well established. Improved outcomes, both radiographically and clinically, have resulted mainly from advances in stem design and improvements in operating techniques. However, there is concern about the durability of bone cement in vivo. We evaluated the physical and chemical properties of CMW1 bone cements retrieved from patients undergoing revision THA.

Methods CMW1 cements were retrieved from 14 patients who underwent acetabular revision because of aseptic loosening. The time in vivo before revision was 7–30 years. The bending properties of the retrieved bone cement were assessed using the three-point bending method. The molecular weight and chemical structure were analyzed by gel permeation chromatography and Fourier-transform infrared spectroscopy. The porosity of the bone cements was evaluated by 3-D microcomputer tomography.

Results The bending strength decreased with increasing time in vivo and depended on the density of the bone cement, which we assume to be determined by the porosity. There was no correlation between molecular weight and time in vivo. The infrared spectra were similar in the retrieved cements and in the control CMW1 cements.

Interpretation Our results indicate that polymer chain scission and significant hydrolysis do not occur in CMW1 cement after implantation in vivo, even in the long term. CMW1 cement was stable through long-term implantation and functional loading.

The concept behind Charnley low-friction arthroplasty was established in the 1960s, and the fundamental principles have remained unchanged since then. Several clinical studies have recently reported the long-term success of total hip arthroplasty (THA). Wroblewski et al. (2009) reported good results using Charnley low-friction arthroplasty with a follow-up of 30–40 years. Overall, 90% of hips were free from pain, and activity was normal in 59% of the patients. Carrington et al. (2009) reported the results of the Exeter Universal cemented femoral component after 15–17 years. With an endpoint of revision for aseptic loosening, the survivorship at 17 years was 100% for the femoral component and 90% for the acetabular component. With all reasons for reoperation as the endpoint, the survivorship was 81%. A variety of cemented stems designed according to various concepts have been used, and several improvements have been incorporated into the operating techniques (Madey et al. 1997, Noble et al. 1998, Scheerlinck and Casteleyn 2006). Although self-curing polymethyl methacrylate (PMMA) bone cements have been used for fixation of the implants for the past 50 years, the composition of the cements has remained essentially unaltered. The ultra-long clinical and radiographic success of cemented THA may depend on the mechanical and chemical longevity of the bone cements in vivo.

Several authors have reported on the in vivo behavior of PMMA bone cement in the implanted joint. Some studies have shown aging of PMMA in vivo. Hughes et al. (2003) showed a decrease in molecular weight and hydrolysis of PMMA associated with long-term implantation. Looney and Park (1986) reported a reduction in flexural strength but not in compressive strength. Fernandez-Fairen and Vazquez (1983) analyzed the compressive properties of the retrieved CMW1 cements and found a decrease in the compressive modulus and strength after long implantation periods. By contrast, Ries et al. (2006) concluded that the most important factor for the mechanical properties of bone cement in vivo is not the implant duration but the porosity. It remains unknown whether the mechanical and chemical properties of bone cement change in vivo, and how these changes affect the long-term outcome of cemented

DOI 10.3109/17453674.2011.625538

THA. We investigated various properties, including molecular weight, chemical structure, bending properties, density, and porosity in retrieved bone cements.

Patients and methods

Sample preparation

CMW1 cements were retrieved from 14 patients who underwent acetabular revision because of aseptic loosening. The median time in vivo before revision was 15 (7–30) years. The retrieved samples were rinsed in saline solution and ethanol, and then stored at room temperature until they were examined.

Molecular weight analysis

The average molecular weight and the molecular weight distribution of the retrieved cements were assessed by gel permeation chromatography (GPC). Molecular weight calibration was established based on polystyrene standards. Briefly, samples were dissolved in tetrahydrofuran (THF) to a concentration of 2 mg/mL at room temperature, and then filtered through 0.45-μm disk filters. Each sample was injected into a 30-cm long GPC gel column (Shodex, Tokyo, Japan) with an inner diameter of 8.0 mm, which was packed with THF with a pore size of 1,000 nm. The injection volume was 50 μL and the flow rate was 1 mL/min at 40°C. A differential refractive index detector (Hitachi L-2000; Hitachi, Tokyo, Japan) was used to monitor changes in the concentration of the sample. The molecular weight distributions of the samples relative to polystyrene were found in terms of the number-averaged molecular weight M_n, the weight-averaged molecular weight M_w, and the polydispersity index (PDI; M_w/M_n ratio).

Fourier-transform infrared spectroscopy (FTIR) analysis

Chemical analysis was performed using FTIR. The FTIR spectra were obtained using a Spectrum BX spectrometer (PerkinElmer, Waltham, MA). All transmission spectra were collected with a spectral resolution of 4 cm^{-1} and spectral range of 4000 to 600 cm^{-1} using KBr pellets. Unimplanted control CMW1 cement specimens were freshly prepared by mixing the powder and liquid components by hand according to the manufacturer's instructions. They were then sent for FTIR analysis within 1 month of preparation.

Bending properties

The retrieved cement specimens were cut and scraped into rectangular specimens (20 mm × 4 mm × 3 mm) using a rotational scraping machine (BUEHLER EcoMet 3000; BUEHLER Ltd., Lake Bluff, IL) with 1–9 specimens for each sample. The bending strength and bending modulus of each retrieved cement specimen and each freshly prepared CMW1 cement specimen were analyzed using an Instron 5500 instrument (Instron, Norwood, MA) at 23 ± 1°C. The crosshead speed and the span were 0.5 mm/min and 15 mm, respectively, when using the 3-point bending method. The values for the bending modulus were derived from the stress-strain curves obtained from the bending tests, as described previously (Shinzato et al. 2002).

Summary of molecular weights for the retrieved cements

Sample no.	Implantation time (years)	M_w (g/mol)	M_n (g/mol)	PDI
1	7	209,737	66,412	3.16
2	7	199,478	68,608	2.91
3	7	220,660	74,217	2.97
4	10	187,296	67,205	2.79
5	10	208,271	64,416	3.23
6	10	217,552	71,617	3.04
7	13	176,996	63,839	2.77
8	13	196,600	67,618	2.91
9	14	192,056	70,209	2.74
10	16	211,157	66,509	3.17
11	21	216,827	62,554	3.47
12	25	203,630	62,005	3.28
13	26	192,270	61,753	3.11
14	30	212,962	66,750	3.19

Porosity analysis

A microfocus X-ray computed tomography system (SMX-100CT-SV3; Shimadzu Co., Kyoto, Japan) was used to acquire microstructural information from the retrieved cements. The entire set of radiographs was deconvoluted by computer software to reconstruct a 3-D image of the microstructure with a voxel size of 16 μm^3. The 3-D data were processed with commercially available 3-D image-processing software (VG Studio MAX 2.0; Volume Graphics, Heidelberg, Germany), and the porosity of the retrieved cements was calculated from the binary material images. The spatial boundary between the pores and the cement was established easily because of the large differences in density.

Statistics

Data from each test were compared by analysis of variance (ANOVA) to determine the overall significance of data trends. For all analyses, $p < 0.01$ was considered significant.

Results

The M_w of the samples ranged from 170,000 to 220,000 g/mol (Table). The molecular weight and PDI did not correlate with the time in vivo ($r = 0.013$, $p = 1.0$; $r = 0.54$, $p = 0.05$, respectively) (Figure 1A and B). Because the molecular weight of the polymer is proportional to the degree of polymerization of the monomer unit, this result suggested that scission of polymer chains did not occur in CMW1

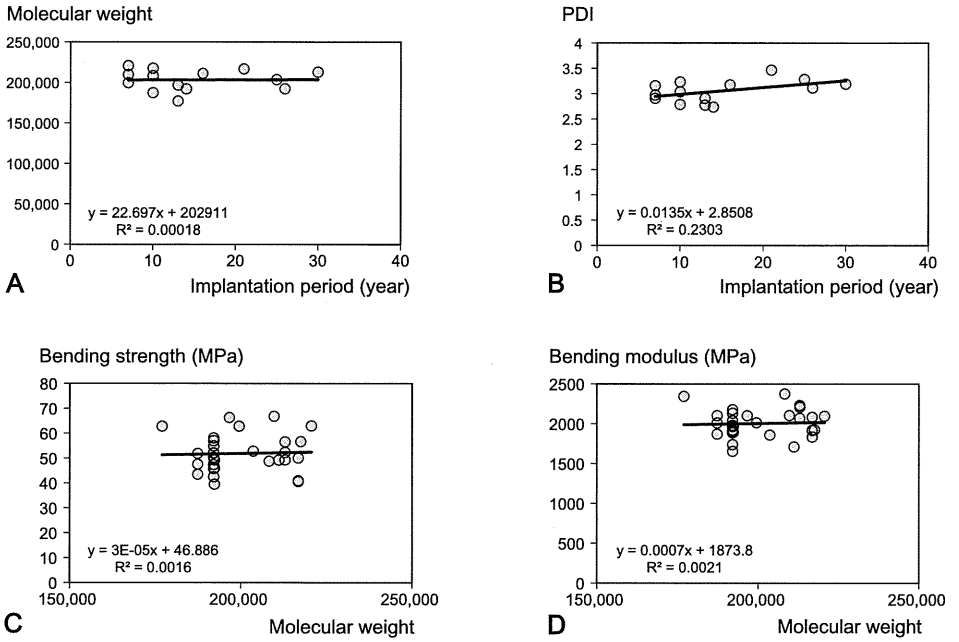

Figure 1 A. Relationship between implantation period and molecular weight. B. Relationship between implantation period and PDI. C. Relationship between molecular weight and bending strength. D. Relationship between molecular weight and bending modulus.

cement in vivo. There was no substantial difference in FTIR spectra between the CMW1 cements in fresh samples after they were cured and in samples retrieved 16 and 30 years after implantation (Figure 2). The spectra of methyl methacrylate homopolymer showed a distinctive absorbance band around 1,730 cm^{-1}, corresponding to the C=O stretch of the ester group (Hughes et al. 2003). This distinctive absorbance band did not differ between freshly prepared and retrieved CMW1 cements. These results indicate that no substantial hydrolysis of the ester group occurred in CMW1 cement in vivo, even after many years.

The molecular weight was not related to the bending strength or the bending modulus ($r = 0.040$, $p = 0.83$; $r = 0.046$, $p = 0.8$, respectively) (Figure 1C and D). By contrast, the bending strength of each cement specimen was reduced with increasing time in vivo, but this was not statistically significant ($r = -0.39$, $p = 0.03$) (Figure 3A). In addition, there was no correlation between bending modulus and the length of the implantation period ($r = -0.038$, $p = 0.8$) (Figure 3B).

The density of the specimens was calculated from their dimension and weight. There was no correlation between the density of the cements and length of time in vivo ($r = -0.20$, $p = 0.3$) (Figure 4A). Density was found to be strongly correlated to bending strength ($r = 0.54$, $p = 0.002$) but not to bending modulus ($r = 0.38$, $p = 0.04$) (Figure 4B and C). There was no correlation between the porosity of the specimens and the time in vivo ($r = 0.27$, $p = 0.1$) (Figure 5A). There was a strong correlation between the density and the porosity of

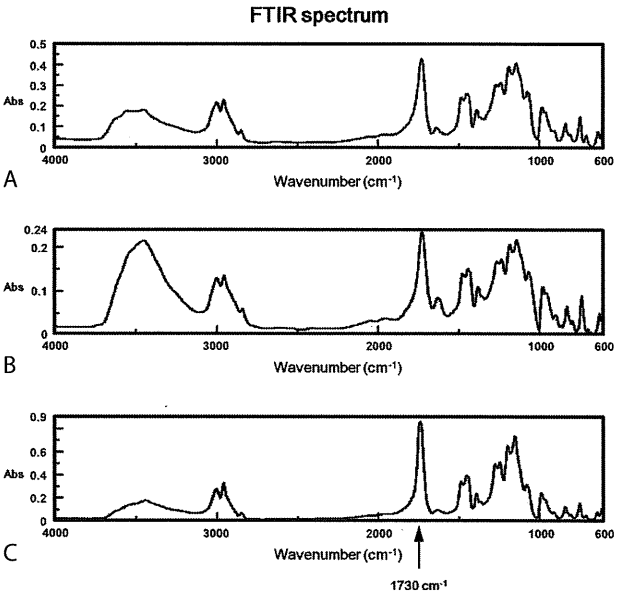

Figure 2. FTIR spectrum of control CMW1 cement (A) and CMW1 cement retrieved 16 years (B) and 30 years (C) after implantation.

the cement ($r = -0.67$, $p < 0.001$) (Figure 5B). The porosity correlated with bending strength ($r = -0.51$, $p = 0.004$) (Figure 5C) but not with bending modulus ($r = -0.18$, $p = 0.4$) (Figure 5D). These results indicate that the porosity of the

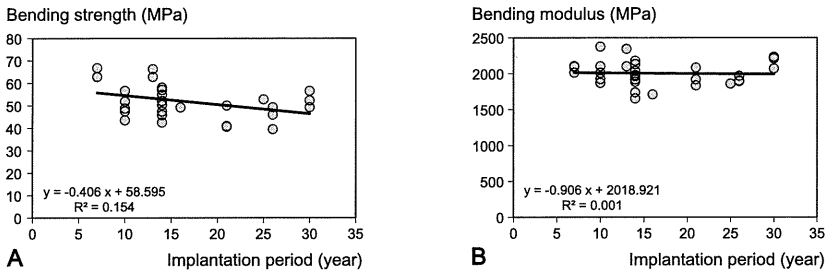

Figure 3. A. Relationship between implantation period and bending strength. B. Relationship between implantation period and bending modulus.

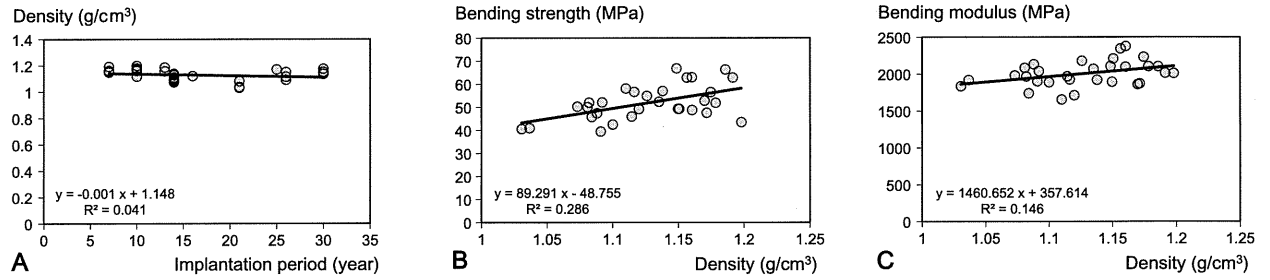

Figure 4. A. Relationship between implantation period and density. B. Relationship between density and bending strength. C. Relationship between density and bending modulus.

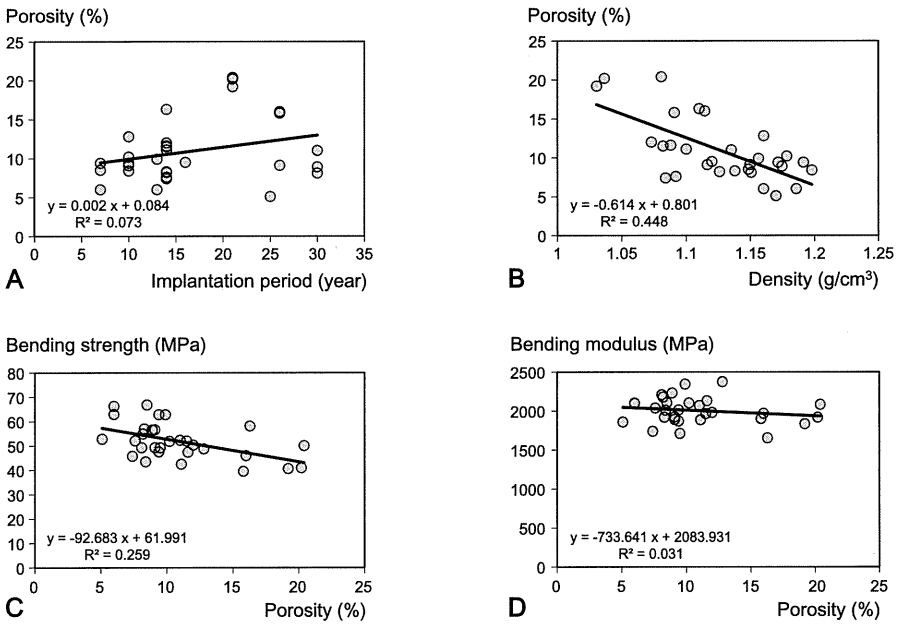

Figure 5. A. Relationship between implantation period and porosity. B. Relationship between density and porosity. C. Relationship between porosity and bending strength. D. Relationship between porosity and bending modulus.

bone cement defined the in vivo mechanical properties of the retrieved specimens. As the porosity of cement is unlikely to change substantially after curing, the mechanical properties of the cement should remain stable.

Discussion

One of the factors that dictate the long-term stability of cemented stems is the longevity of the cement itself. Failure of the cemented stem implanted in THAs is induced by excessive stress in the cement mantle, leading to micromovement of the stem and debonding at the cement-stem interface, along with microcracking in the cement (Gardiner and Hozack 1994, Ong et al. 2002). This cement damage finally causes stem loosening, stem subsidence, increased production of wear particles, and osteolysis. Thus, retention of the chemical and mechanical properties of the bone cement in vivo is critical for achievment of long-term success in THA.

Although previous studies have used various tests to investigate the in vivo behavior and chemical and mechanical properties of bone cements, there is no consensus on the aging of the cement (Fernandez-Fairen and Vazquez 1983, Looney and Park 1986, Hughes et al. 2003, Ries et al. 2006). The molecular structure, the dispersity of the contrast medium, or the distribution of pores introduced during the preparation of bone cements may affect their mechanical properties, and these complex factors make interpretation of the data—and comparison between studies—difficult.

The mechanical properties of implanted bone cements depend on the chemistry of the bone cement and on the mixing method (Lewis 1997). Our study shows that there is no correlation between the molecular weight of the bone cement and the time in vivo, and that neither degradation of the main chain nor hydrolysis of PMMA occurs in CMW1 cement. We also found no relationship between molecular weight and bending strength or bending modulus. Our results contrast with those of Hughes et al. (2003), who found a decrease in molecular weight and chemical degradation in retrieved Simplex P and Palacos R cements that had aged up to 23 years in vivo. CMW1 powder comprises only methyl methacrylate, whereas Palacos R powder contains methylacrylate, which is polar and hydrophilic. Simplex P contains hydrophobic styrene comonomer, which has no polarity. In vivo degradation of bone cements is related to particular combinations of localized acidic pH, free radical oxidation induced by superoxidizing substances, and hydrolyzing enzymes. One possible explanation of these results (Hughes et al. 2003) that the differences in chemical properties of bone cements confer different sensitivities to biological processes that induce degradation. The cements retrieved from total knee arthroplasties after similar in vivo aging times to those from THAs showed little change in their structural properties, suggesting that in vivo degradation of the bone cements is related to the biological response to the implant and the local environment of the joint (Hughes et al. 2003). These lines of evidence strongly suggest that the degradation of bone cements in vivo depends partly on the environment of implantation and partly on the composition of bone cements. In addition, the FTIR spectra showed an increase in the large band at 3,500 cm-1, attributable to OH stretching in water, in some retrieved specimens. Water is a plasticizer for methacrylate, and could therefore reduce the mechanical properties of bone cement. This should be clarified by further studies.

Although Dall et al. (2007) reported that inter-batch and intra-batch variability was seen in the viscosity of all brands of bone cement, the strong relationship between bending strength and density or porosity shows that the mechanical properties of bone cements depend on their density or porosity (Weinstein et al. 1976, Wang et al. 1993, Chaplin et al. 2006). Our study and studies of others have shown significant correlations between density and porosity. High porosity contributes to microcracks in the bone cement, which lead to release of PMMA particles and induce aseptic loosening and osteolysis (James et al. 1992, Graham et al. 2003, Hoey et al. 2009). In addition, cracks and voids could be also generated by micromovement between cement and prosthesis/bone or by wear, and may affect the mechanical properties. Thus, the porosity of bone cement is a critical factor in determining the mechanical properties of the bone cement in vivo. The porosity of bone cement is determined by the method used to prepare and apply it. In the modern cementing technique, vacuum mixing reduces the porosity of bone cement and improves its fatigue resistance (James et al. 1992, Wang et al. 1993). Graham et al. (2000) reported that the internal porosity of bone cement is greatly reduced by vacuum mixing, whereas a higher porosity introduced during the hand-mixing process caused all hand-mixed specimens to have inferior fracture and fatigue resistance to their vacuum-mixing counterparts. Moreover, elevated pressure during curing helps reduce the porosity of the bone cement; thus, high-pressure insertion of implants substantially improves the mechanical properties of the bone cement (Bayne et al. 1975, Apostolou et al. 2007). Taken together, this evidence shows that the mechanical properties of implanted bone cement depend on the operating techniques rather than the period of implantation.

Ries et al. (2006) investigated the variables fracture toughness, porosity, molecular weight, and time in vivo of the bone cement, and concluded that porosity and fracture toughness are significantly and inversely related. All bone cements retrieved in the acetabular reconstruction in our study were hand-mixed and were applied to the acetabulum without use of a cement pressurizer. One possible reason that the porosity increases in relation to the time in vivo is that cement pressurization in the implantation of the acetabular component has been improved by the development of operation instruments, including the component holder and component pusher, which reduce the initial porosity of the bone cement. These lines of evidence also suggest that the mechanical properties of bone cement in vivo are strongly affected by the cementing techniques.

In conclusion, we found that the properties of bone cement were determined by the porosity of the cement but were not affected by the length of the period of implantation. The chemical structure of CMW1 cement was stable in vivo even after more than 20 years.

HO performed the experiments and participated in writing of the manuscript. HA coordinated the study, participated in design of the protocol, performed the experiments, analyzed the data, and participated in writing of the manuscript. MT analyzed the data and participated in writing of the manuscript. TK performed the experiments and analyzed the data. KY analyzed the data. TY participated in design of the protocol. HO participated in design of the protocol and prepared the samples. TN obtained funding and participated in design of the protocol.

No competing interests declared.

Apostolou C D, Yiannakopoulos C K, Ioannidis T T, Papagelopoulos P J, Korres D. Mechanical stability of total hip replacement using pressurization of bone cement during curing: push-out tests in cadaver femora. Orthopedics 2007; 30 (12): 1028-32.

Bayne S C, Lautenschlager E P, Compere C L, Wildes R. Degree of polymerization of acrylic bone cement. J Biomed Mater Res 1975; 9 (1): 27-34.

Carrington N C, Sierra R J, Gie G A, Hubble M J, Timperley A J, Howell J R. The Exeter Universal cemented femoral component at 15 to 17 years: an update on the first 325 hips. J Bone Joint Surg (Br) 2009; 91 (6): 730-7.

Chaplin R P, Lee A J, Hooper R M, Clarke M. The mechanical properties of recovered PMMA bone cement: a preliminary study. J Mater Sci Mater Med 2006; 17 (12): 1433-48

Dall G F, Simpson P M, Mackenzie S P, Breusch S J. Inter- and intra-batch variability in the handling characteristics and viscosity of commonly used antibiotic-loaded bone cements. Acta Orthop 2007; 78 (3): 412-20

Fernandez-Fairen M, Vazquez J J. The aging of polymethyl methacrylate bone cement. Acta Orthop Belg 1983; 49 (4): 512-20.

Gardiner R C, Hozack W J. Failure of the cement-bone interface. A consequence of strengthening the cement-prosthesis interface? J Bone Joint Surg (Br) 1994; 76(1): 49-52.

Graham J, Pruitt L, Ries M, Gundiah N. Fracture and fatigue properties of acrylic bone cement: the effects of mixing method, sterilization treatment, and molecular weight. J Arthroplasty 2000; 15 (8): 1028-35.

Graham J, Ries M, Pruitt L. Effect of bone porosity on the mechanical integrity of the bone-cement interface. J Bone Joint Surg (Am) 2003; 85 (10): 1901-8.

Hoey D, Taylor D. Quantitative analysis of the effect of porosity on the fatigue strength of bone cement. Acta Biomater 2009; 5 (2): 719-26

Hughes K F, Ries M D, Pruitt L A. Structural degradation of acrylic bone cements due to in vivo and simulated aging. J Biomed Mater Res A 2003; 65 (2): 126-35.

James S P, Jasty M, Davies J, Piehler H, Harris W H. A fractographic investigation of PMMA bone cement focusing on the relationship between porosity reduction and increased fatigue life. J Biomed Mater Res 1992; 26 (5): 651-62.

Lewis G. Properties of acrylic bone cement: state of the art review. J Biomed Mater Res 1997; 38 (2): 155-82.

Looney M A, Park J B. Molecular and mechanical property changes during aging of bone cement in vitro and in vivo. J Biomed Mater Res 1986; 20 (5): 555-63.

Madey S M, Callaghan J J, Olejniczak J P, Goetz D D, Johnston R C. Charnley total hip arthroplasty with use of improved techniques of cementing. The results after a minimum of fifteen years of follow-up. J Bone Joint Surg (Am) 1997; 79 (1): 53-64.

Noble P C, Collier M B, Maltry J A, Kamaric E, Tullos H S. Pressurization and centralization enhance the quality and reproducibility of cement mantles. Clin Orthop 1998; (355): 77-89.

Ong A, Wong K L, Lai M, Garino J P, Steinberg M E. Early failure of precoated femoral components in primary total hip arthroplasty. J Bone Joint Surg (Am) 2002; 84 (5): 786-92.

Ries M D, Young E, Al-Marashi L, Goldstein P, Hetherington A, Petrie T, Pruitt L. In vivo behavior of acrylic bone cement in total hip arthroplasty. Biomaterials 2006; 27 (2): 256-61.

Scheerlinck T, Casteleyn P P. The design features of cemented femoral hip implants. J Bone Joint Surg (Br) 2006; 88 (11): 1409-18.

Shinzato S, Nakamura T, Ando K, Kokubo T, Kitamura Y. Mechanical properties and osteoconductivity of new bioactive composites consisting of partially crystallized glass beads and poly(methyl methacrylate). J Biomed Mater Res 2002; 60 (4): 556-63

Wang J S, Franzen H, Jonsson E, Lidgren L. Porosity of bone cement reduced by mixing and collecting under vacuum. Acta Orthop Scand 1993; 64 (2): 143-6.

Weinstein A M, Bingham D N, Sauer B W, Lunceford E M. The effect of high pressure insertion and antibiotic inclusion upon the mechanical properties of polymethylmethacrylate. Clin Orthop 1976; (121): 67-73.

Wroblewski B M, Siney P D, Fleming P A. Charnley low-frictional torque arthroplasty: follow-up for 30 to 40 years. J Bone Joint Surg (Br) 2009; 91 (4): 447-50.

J Orthop Sci (2011) 16:26–37
DOI 10.1007/s00776-010-0007-1

ORIGINAL ARTICLE

A novel technique for impaction bone grafting in acetabular reconstruction of revision total hip arthroplasty using an ex vivo compaction device

Haruhiko Akiyama · Takkan Morishima · Mitsuru Takemoto · Koji Yamamoto · Hiromi Otsuka · Toshiki Iwase · Tamon Kabata · Tsunemitsu Soeda · Keiichi Kawanabe · Keiji Sato · Takashi Nakamura

Received: 19 May 2010 / Accepted: 7 September 2010 / Published online: 22 January 2011

Abstract

Background Impaction bone grafting allows restoration of the acetabular bone stock in revision hip arthroplasty. The success of this technique depends largely on achieving adequate initial stability of the component. To obtain well-compacted, well-graded allograft aggregates, we developed an ex vivo compaction device to apply it in revision total hip arthroplasty on the acetabular side, and characterized mechanical properties and putative osteoconductivity of allograft aggregates.

Methods Morselized allograft bone chips were compacted ex vivo using the creep technique and subsequent impaction technique to form the bone aggregates. Impaction allograft reconstruction of the acetabulum using an ex vivo compaction device was performed on eight hips. The mechanical properties and three-dimensional micro-CT-based structural characteristics of the bone aggregates were investigated.

Results In clinical practice, this technique offered good reproducibility in reconstructing the cavity and the segmental defects of the acetabulum, with no migration and no loosening of the component. In vitro analysis showed that the aggregates generated from 25 g fresh-frozen bone chips gained compression stiffness of 13.5–15.4 MPa under uniaxial consolidation strain. The recoil of the aggregates after compaction was 2.6–3.9%. The compression stiffness and the recoil did not differ significantly from those measured using a variety of proportions of large- and small-sized bone chips. Micro-CT-based structural analysis revealed average pore sizes of 268–299 μm and average throat diameter of pores in the bone aggregates of more than 100 μm. These sizes are desirable for osteoconduction, although large interconnected pores of more than 500 μm were detectable in association with the proportion of large-sized bone chips. Cement penetration into the aggregates was related to the proportion of large-sized bone chips.

Conclusion This study introduces the value of an ex vivo compaction device in bone graft compaction in clinical applications. In vitro analysis provided evidence that compaction of sequential layers of well-compacted, well-graded bone aggregates, i.e., the aggregates comprising smaller sized chips at the host bone side and larger sized chips at the component side, may have the advantages of initial stability of the acetabular component and biological response of the grafted aggregates.

H. Akiyama (✉) · M. Takemoto · K. Yamamoto · T. Soeda · T. Nakamura
Department of Orthopaedics, Kyoto University,
54 Shogoin-Kawahara cho, Sakyo, Kyoto 606-8507, Japan
e-mail: hakiyama@kuhp.kyoto-u.ac.jp

T. Morishima · H. Otsuka · K. Sato
Department of Orthopaedics, Aichi Medical University,
Nagakute, Aichi 480-1195, Japan

T. Iwase
Department of Orthopaedics, Hamamatsu Medical Center,
328 Tomitsuka-cho, Naka-ku, Hamamatsu,
Shizuoka 432-8580, Japan

T. Kabata
Department of Orthopaedics, Kanazawa University,
13-1 Takaramachi, Kanazawa, Ishikawa 920-0934, Japan

K. Kawanabe
Department of Orthopaedics, Kobe City Medical Center General Hospital, 4-6, Minatojimanakamachi, Chuo-ku, Kobe,
Hyogo 650-0046, Japan